# CANADIAN THESES

# THÈSES CANADIENNES

## NOTICE

The quality of this microfiche is heavily dependent upon the quality of the original thesis submitted for microfilming. Every effort has been made to ensure the highest quality of reproduction possible.

If pages are missing, contact the university which granted the degree.

Some pages may have indistinct print especially if the original pages were typed with a poor typewriter ribbon or if the university sent us an inferior photocopy.

Previously copyrighted materials (journal articles, published tests, etc.) are not filmed.

Reproduction in full or in part of this film is governed by the Canadian Copyright Act, R.S.C. 1970, c. C-30.

## AVIS

La qualité de cette microfiche dépend grandement de la qualité de la thèse soumise au microfilmage. Nous avons tout fait pour assurer une qualité supérieure de reproduction

S'il manque des pages, veuillez communiquer avec l'université qui a conféré le grade.

La qualité d'impression de certaines pages peut laisser à désirer, surtout si les pages originales ont été dactylographiées à l'aide d'un ruban usé ou si l'université nous a fait parvenir une photocopie de qualité inférieure

Les documents qui font déjà l'objet d'un droit d'auteur (articles de revue, examens publiés, etc ) ne sont pas microfilmés.

La reproduction, même partielle, de ce microfilm est soumise à la Loi canadienne sur le droit d'auteur, SRC 1970, c. C-30.

## THIS DISSERTATION HAS BEEN MICROFILMED EXACTLY AS RECEIVED

## LA THÈSE A ÉTÉ MICROFILMÉE TELLE QUE NOUS L'AVONS REÇUE

# Shock and Pressure Amplification in a Stepped Hartmann-Sprenger Tube

Barbara Boloz-Skarzynska

A Thesis

in

The Department

of

Mechanical Engineering

Presented in Partial Fulfillment of the Requirements
for the Degree of Master of Engineering at
Concordia University
Montréal, Québec, Canada

July 1987

ISBN 0-315-37077-7

# ABSTRACT

## Shock and Pressure Amplification in a Stepped Hartmann-Sprenger Tube

Barbara Boloz-Skarzynska

A combined theoretical and experimental study was conducted to determine both pressure and shock amplification in a stepped Hartmann-Sprenger tube. The method of characteristics was imployed to determine the flow dynamics and to construct the appropriate wave diagrams. Detailed pressure measurements were carried out up to diameter ratios of 4 and for a jet Mach number ranging between 0.4 and 1. Flow visualization inside the tube was obtained via spark schlieren photography taken at different time intervals during the resonant cycle. Experimental results are found to agree well with those obtained theoretically. Both theory and experiments show a decrease in the amplification of the pressure's amplitude $\Delta P_R$ with the increase in Jet Mach number. For sonic jets, and for large diameter ratios, the pressure amplitude is found to be 1.89 times higher that obtained from a constant area tube.

# ACKNOWLEDGEMENTS

The author wishes to express her gratitude to Professor R.A. Neemeh for the constant encouragement he provided throughout the course of this work; his many helpful suggestions for improving the text and also the valuable discussions which helped along to clarify numerous points in this work.

Thanks are also due to Mrs. Christine Nadeau for her effort in proofreading and typing this report.

Also to be mentioned is the support of the Natural Sciences and Engineering Research Council of Canada under Grant No. A-4206.

# TABLE OF CONTENTS


| | Page |
|---|---|
| ABSTRACT | iii |
| ACKNOWLEDGEMENTS | iv |
| LIST OF FIGURES | vii |
| LIST OF TABLES | ix |
| NOMENCLATURE | x |
| Chapter 1 | |
| INTRODUCTION | 1 |
| Chapter 2 | |
| THEORETICAL ANALYSIS | 4 |
| 2.1 The Simple H-S Tube | 4 |
| 2.1.1 Description of the Flow Field | 4 |
| 2.1.2 Simplified Wave Diagram | 6 |
| 2.2 Flow in the Stepped H-S Tube | 8 |
| 2.2.1 Description of the Flow Field | 8 |
| 2.2.2 Simplified Wave Diagram | 9 |
| 2.3 Boundary Conditions | 12 |
| 2.3.1 Inflow | 12 |
| 2.3.2 Outflow | 13 |
| Chapter 3 | |
| EXPERIMENTAL APPARATUS | 15 |
| Chapter 4 | |
| EXPERIMENTAL RESULTS | 17 |
| 4.1 Flow Visualization in a Stepped Tube | 17 |
| 4.2 Pressure measurement for Variable D1/D2 Ratio | 19 |

Page

Chapter 5

THEORETICAL RESULTS . . . . . 22

5.1 Pressure Amplification for Large Area Contraction . . . . . 22

5.1.1 Regions 2 and 3 . . . . . 22

5.1.2 Regions 3 and * . . . . . 22

5.1.3 Regions 3, 6 and 7 . . . . . 23

5.1.4 Regions 7 and 8 . . . . . 23

5.1.5 Regions 8 and 10 . . . . . 23

5.2 Pressure Amplification for Small Area Contraction . . . . . 25

5.3 Detailed Wave Diagram for $M_j = 0.6$ and Diameter Ratios of 1.34, 2 and 4 . . . 27

5.3.1 Case 1 . . . . . 27

5.3.2 Case 2 . . . . . 28

Chapter 6

FREQUENCY OF OSCILLATIONS . . . . . 30

6.1 Frequency of Oscillation for the Simple H-S Tube . . . . . 30

6.2 Frequency of Oscillations for the Stepped Tube and Different Diameter Ratios . . . 32

6.3 Frequency of Oscillations for the Large Area Contraction (D1/D2 → ∞) . . . . . 33

Chapter 7

SUMMARY AND CONCLUSIONS . . . . . 36

REFERENCES . . . . . 39

## CAPTION OF FIGURES


| | | Page |
|---|---|---|
| Figure 1 | The resonance tubes | 41 |
| Figure 2 | Typical variation of stagnation pressure in an underexpanded periodic jet | 42 |
| Figure 3 | The resonant cycle within the simple H-S tube | 43 |
| Figure 4 | Detailed wave diagram for the simple tube | 44 |
| Figure 5 | Simplified wave diagram for the simple tube | 45 |
| Figure 6 | A detailed wave diagram for the simple tube | 46 |
| Figure 7 | The pressure history at the closed end of the H-S tube for $M_s$ = 0.77 | 47 |
| Figure 8 | The resonance cycle within the stepped H-S tube | 48 |
| Figure 9 | Simplified wave diagram for the stepped tube | 49 |
| Figure 10 | Wave interactions at the area discontinuity | 50 |
| Figure 11 | Boundary conditions at the open end | 51 |
| Figure 12 | Experimental apparatus | 52 |
| Figure 13 | The 50 x 50 mm square shock tube and auxiliary equipments | 53 |
| Figure 14 | A set of spark schlieren photographs of the flow inside a double step H-S tube | 54 |
| Figure 15 | Pressure histories for an H-S tube with and without area contraction | 55 |
| Figure 16 | Pressure amplitude as a function of the diameter ratio $D_1/D_2$, for different $M_j$ | 56 |
| Figure 17 | Wave diagram for the large area contraction, $D_1/D_2 \to \infty$ | 57 |
| Figure 18 | Pressure amplitude as a function of the jet Mach number for the large area contraction | 58 |
| Figure 19 | Wave diagram for the small area contraction | 59 |
| Figure 20 | Pressure amplitude as a function of the diameter ratio $D_1/D_2$ for the small area contraction | 60 |

| | | Page |
|---|---|---|
| Figure 21 | Typical wave diagram, $M_j = 0.6$ and $D_1/D_2 = 1.33$ | 61 |
| Figure 22 | Pressure amplitude as a function of diameter ratio $D_1/D_2$, $L_1/L_2 = 1$ | 62 |
| Figure 23 | Pressure amplitude as a function of diameter ratio $D_1/D_2$ for different length ratios $L_1/L_2$ | 63 |
| Figure 24 | Simplified wave diagram and the pressure history for $M_j = 0.6$, $D_1/D_2 = 4$ and $L_1/L_2 = 1.25$ | 64 |
| Figure 25 | Simplified wave diagram and the pressure history for $M_j = 0.6$, $D_1/D_2 = 4$ and $L_1/L_2 = 1$ | 65 |
| Figure 26 | Wave diagram for frequency calculation for simple tube | 66 |
| Figure 27 | Frequency of oscillations for the simple tube versus the jet Mach number | 67 |
| Figure 28 | Wave diagram used for frequency calculation | 68 |
| Figure 29 | Frequency of oscillations for the stepped tube versus diameter ratio $D_1/D_2$, $M_j = 0.6$ | 69 |
| Figure 30 | Wave diagram for frequency calculations for tubes with large area contractions | 70 |
| Figure 31 | Frequency of oscillations versus the jet Mach number for large area contractions | 71 |

## CAPTION OF TABLES


| | | Page |
|---|---|---|
| Table 1 | The pressure amplitude for different diameter ratios and different jet Mach numbers | 72 |
| Table 2 | The pressure amplitude as a function of diameter ratio for $M_j = 0.6$ | 72 |
| Table 3 | The pressure amplitude as a function of the length ratio for different diameter ratios and $M_j = 0.6$ | 73 |
| Table 4 | The values of flow Mach number and sound speed for $M_j = 0.6$, $D_1/D_2 = 4$ and $L_1/L_2 = 1.25$ | 73 |
| Table 5 | The values of flow Mach number and sound speed for $M_j = 0.6$, $D_1/D_2 = 4$ and $L_1/L_2 = 1$ | 74 |
| Table 6 | Frequency of oscillations for the simple H-S tube and different jet Mach numbers | 74 |
| Table 7 | Frequency of oscillations for $M_j = 0.6$ and different diameter ratio | 75 |
| Table 8 | Frequency of oscillations for different jet Mach numbers and large area contraction, $D_1/D_2 \to \infty$ | 75 |

## NOMENCLATURE

$a$ = speed of sound

$a_a$ = ambient speed of sound

$a_j$ = jet sound speed at the nozzle exit

$a_{max}$ = maximum speed of sound

$a_{min}$ = minimum speed of sound

$A$ = cross section area of the tube

$D_1$ = diameter of upstream tube

$D_2$ = diameter of downstream tube

$L_1$ = length of the upstream section of the tube

$L_2$ = length of the downstream section of the tube

$L$ = total length of the tube ($L_1 + L_2$)

$L_s$ = length of the constant area tube

$f$ = frequency of oscillations

$f_o$ = acoustical frequency of oscillations of the total tube length ($a_a/4L$)

$f_s$ = frequency of oscillations for the constant area tube

$\dot{m}$ = mass flow rate

$M_j$ = jet Mach number

$M$ = flow Mach number

$M_s$ = shock Mach number

$p$ = static pressure

$p_a$ = ambient pressure

$p_j$ = static pressure of nozzle-jet

$p_{0j}$ = total pressure of nozzle-jet

$\Delta p$ = pressure amplitude $p_{max} - p_{min}$

$\Delta p_R$ = ratio between $\Delta p$ for the tube with area contraction and constant area one

$P, Q$ = Riemman variables

$R$ = gas constant

$t$ = time

$t_p$ = period of oscillation

$T$ = static temperature of the flow

$T_0$ = total temperature of the flow

$u$ = flow velocity

$u_j$ = jet velocity at the nozzle exit

$V$ = average velocity of the wave

$x$ = distance

$\rho$ = gas density

$\gamma$ = specific heat ratio

$\tau$ = nondimensional time ($a_j t / L$)

# Chapter 1

## INTRODUCTION

The Hartmann-Sprenger tube [1,2] consists of a tube, closed at one end, with its open end facing an exciting jet. (Figure 1).

The discovery of the resonance phenomenon was made by Hartmann in 1919, while measuring the stagnation pressure distribution along the axis of an underexpanded periodic jet [3]. Hartmann investigated this phenomenon further, using a short tube, of length to diameter ratio up to 4. From his investigations it was concluded that, in order to maintain the oscillations, the mouth of the tube should be located in one of the regions of instability (i.e.: the regions where the pitot pressure increases with the distance from the nozzle). (Figure 2).

Resonant oscillations in tubes excited by subsonic or straight supersonic jets were discovered by Sprenger. To maintain the oscillations it was necessary to weaken the center core of the jet by placing a fine wire across the nozzle plane. The resonant oscillations obtained in such a way were essentially similar to those caused by periodic jets.

In acknowledgement of the fundamental work done by the above two investigators, the resonance tube was named the Hartmann-Sprenger tube (H-S tube).

The Hartmann-Sprenger tube has attracted the attention of many other experimenters who either investigated the physical problems concerning its mechanism of operation or developed some of its practical, industrial applications.

The thermal phenomenon of the resonance tube was also discovered by Sprenger. During the oscillations, the temperature of the gas at the closed end of the tube rose rapidly to values far exceeding the stagnation temperature of the jet. This thermal effect was attributed to the internal travelling shock waves, which were continuously heating the indigenous fluid, (i.e.: the fluid that remains permanently in the tube). For a tube of length to diameter ratio of 34, and a reservoir pressure of 5 atm, Sprenger was able to reach temperatures higher than 1000°C [2]. The device was later classified by Stabinsky et al [4] as a possible igniter for various fuel mixtures and explosives.

Rakowsky et al [5,6] employed various geometric shapes and a wide range of gases. Helium gas and the stepped tube were found to be the best combination to produce temperatures as high as 1500°K in less than 0.1 s. Logarithmic spirals area contraction was also preferred over the tapered one [7].

An axisymmetric device, first introduced in 1974 by Wu et al [8], produced repeated implosions. Unfortunately, symmetrical implosions were impossible to produce, thus limiting temperatures to finite values. Later, a subsonic model was introduced by Neemeh et al [9], where a much

improved symmetry and higher temperatures were obtained.

The stepped tube was under investigation in the past decade by Brocher et al [10,11], due to its simplicity and ability to produce high temperatures. Detailed experimental results were reported, but the theory employed was limited to just accoustic approximations where no quantitative results could be obtained. No conclusive results, concerning the mechanism of oscillations, nor the maximum pressure amplitude and its relationship to shock strength, were reported.

The objective of the present work is therefore to analyse the wave motion inside the stepped tube. This will be acomplished, experimentally, via flow visualization and pressure measurement, and theoretically, by the use of the method of characteristics, taking into account both wave reflection and pressure variations across the area of discontinuity.

# Chapter 2

# THEORETICAL ANALYSIS

## 2.1 The Simple H-S Tube

### 2.1.1 Description of the Flow Field

The resonant cycle for the simple H-S tube, excited by a subsonic jet, can be divided into four phases. (Figure 3).

Temporary Steady Flow

The inflow starts when the subsonic jet from the nozzle flows into the tube. Since the stagnation pressure of the jet is higher than the pressure inside the tube, an incident shock wave forms near the mouth of the tube. The shock travels downstream, thus increasing the pressure within the tube (3a). After reflection from the closed end, the shock travels towards the open end, bringing the fluid behind the shock to rest at higher pressures (3b). At the same time, inflow steadily increases until the shock reaches the open end.

Transition from Inflow to Outflow

Transition from inflow to outflow occurs very suddenly as soon as the internal shock leaves the tube. A centered expansion fan forms and propagates into the tube.

Outflow

Outflow is maintained at approximately constant conditions (3c) until the expansion waves reflect from the closed end (3d) and reach the open end, bringing the

pressures to lower values.

Transition from Outflow to Inflow

Transition from outflow to inflow is more gradual. Outflow velocities decrease with the arrival of the reflected expansion waves until inflow starts, thus driving an internal shock propagating downstream and the cycle repeats as before.

During the periodic motion part of the fluid (the indegenous fluid) remains permanently in the tube. The other part is called "extraneous fluid" as it enters the tube during inflow and comes out during outflow.

For the analysis of the unsteady, one dimensional flow within the tube, the method of characteristics is used. Without any appropriate assumptions, computation by this method could be time consuming and laborious. For simplification the following 7 assumptions are made:

(1) Motion in the tube is strictly one dimensional
(2) Viscous effects are negligible
(3) The flow is isentropic
(4) The tube is completely insulated and the heat capacity of the tube is neglected
(5) Internal shock ($M_s<2$) is replaced by a compression wave
(6) Centered expansion waves are replaced by a single expansion wave
(7) For the graphical representation all waves are assumed linear and moving at the same speed

In Figure 4, a detailed wave diagram is presented. The corresponding simplified one is shown in Figure 5 where it is seen that one cycle consists of four different regions (1,2,3,4), bounded by shock waves or expansion waves. The distances AB and BC represent the time during which the inflow and outflow take place.

2.1.2 Simplified Wave Diagram

Assuming full inflow and outflow as boundary conditions, the pressure amplitude for the simple H-S tube can be obtained as follows:

-According to Figure 6.

Regions 1 and 2

$P_1 = P_2$, i.e.

$$u_j + \frac{2}{\gamma-1} a_j = u_2 + \frac{2}{\gamma-1} a_2 \quad \text{where } u_2=0, \text{ so}$$

$$\frac{a_2}{a_j} = 1 + \frac{\gamma-1}{2} M_j \tag{1a}$$

and

$$\frac{p_2}{p_j} = \left(1 + \frac{\gamma-1}{2} M_j\right)^{\frac{2\gamma}{\gamma-1}} \tag{1b}$$

Regions 2 and 3

$Q_2 = Q_3$, i.e.

$$-u_2 + \frac{2}{\gamma-1} a_2 = -u_3 + \frac{2}{\gamma-1} a_3 \quad \text{where } u_2 = 0$$

and assuming full expansion to $p_a = p_j$, $a_3 = a_j$, so $u_3 = -u_j$.

Regions 3 and 4

$P_3 = P_4$, i.e.

$$-u_j + \frac{2}{\gamma-1} a_j = u_4 + \frac{2}{\gamma-1} a_4 \quad \text{where } u_4 = 0, \text{ so that}$$

$$\frac{a_4}{a_j} = 1 - \frac{\gamma-1}{2} M_j \tag{2a}$$

and

$$\frac{p_4}{p_j} = \left(1 - \frac{\gamma-1}{2} M_j\right)^{\frac{2\gamma}{\gamma-1}} \tag{2b}$$

The difference between maximum and minimum pressures in the tube is

$$\frac{p_{max} - p_{min}}{p_j} = \frac{p_4 - p_2}{p_j} = \frac{\Delta p}{p_j}$$

$$\frac{\Delta p}{p_j} = \left(1 + \frac{\gamma-1}{2} M_j\right)^{\frac{2\gamma}{\gamma-1}} - \left(1 - \frac{\gamma-1}{2} M_j\right)^{\frac{2\gamma}{\gamma-1}} \tag{3}$$

For the small jet Mach number (i.e.: $M_j = 1$), after expansion in the series, one can obtain

$$\frac{\Delta p}{p_j} = 1 + \gamma M_j - 1 + \gamma M_j = 2 \gamma M_j \tag{4}$$

In Figure 7, the pressure history for the closed end of the tube is shown. The experimental results were obtained by Wu et al [12].

## 2.2 Flow in the Stepped H-S Tube

### 2.2.1 Description of the Flow Field

In the case of the stepped H-S tube, the description of the flow field within the tube is much more complicated. However, the resonant cycle can also be divided into four phases. (Figure 8).

Temporary Steady Inflow

During which an internal shock wave forms and propagates into the tube (8a). The interaction of the shock with the area contraction results in a transmitted wave and a reflected one (8b). During the passage of the two compression waves in opposite directions, the fluid from the larger part of the tube is flowing to the narrower one.

Transition from Inflow to Outflow

After the reflected shock reaches the open end, the flow behind it is at relatively high pressures and as soon as it leaves the tube, an expansion wave forms, thus switching inflow to outflow.

Outflow

While the expansion wave is propagating downstream along the tube, the transmitted shock wave reflects from the closed end and propagates upstream (8c). Meanwhile the direction of the flow in the area contraction remains the same.

Collision of the two oncoming waves at the area contraction results in two expansion propagating in opposite

directions, changing the direction of the flow between the two parts of the tube (8d).

Transition from Outflow to Inflow

When the expansion wave reaches the open end, inflow starts and the cycle repeats (8e).

The pattern described is one of the easiest that can be obtained with the stepped resonant tube. Usually, the situation after collision of the incidental expansion wave with the reflected shock wave at the area of contraction, could not be foreseen without calculation (8d). Both waves going in opposite directions after collision could be either compression or expansion ones, depending on the conditions on both sides of the area of discontinuity.

2.2.2 Simplified Wave Diagram

Using all the assumptions previously described, the simplified wave diagram for the flow within the stepped tube can be constructed with the help of the method of characteristics. A typical wave diagram is shown in Figure 9.

For the graphical representation, all waves are assumed to move with the same speed; however, the actual ones were calculated point by point in the wave diagram. The latter was constructed for various initial conditions and the calculations continued until steady state operation was reached. At the region of discontinuity, solution was obtained by iteration for every incoming wave. Steady solution to the flow was used to relate the flow conditions on both sides of

the area of contraction.

Knowing conditions 3 and 4 behind the incoming P and Q waves, respectively, (Figure 10), the solutions to points 5 and 6 were obtained as follows:

Regions 3 and 5

$$P_3 = P_5, \text{ i.e.}$$

$$u_3 + \frac{2}{\gamma-1} a_3 = u_5 + \frac{2}{\gamma-1} a_5, \quad \text{or}$$

$$(M_3 + \frac{2}{\gamma-1})a_3 = (M_5 + \frac{2}{\gamma-1})a_5 \quad \text{where } M = \frac{u}{a} \qquad (5)$$

Regions 4 and 6

$$Q_4 = Q_6, \text{ i.e.}$$

$$-u_4 + \frac{2}{\gamma-1} a_4 = -u_6 + \frac{2}{\gamma-1} a_6, \quad \text{or}$$

$$(-M_4 + \frac{2}{\gamma-1})a_4 = (-M_6 + \frac{2}{\gamma-1})a_6 \qquad (6)$$

Regions 5 and 6 are related by the steady isentropic flow equations. The flow between them is similar to that in a convergent nozzle.

Assuming $M_5$, $a_5$ can be calculated from Equation (5). Knowing geometry of the duct, one can obtain $a_6$ and $M_6$ using the following simple relations:

- between areas

$$\frac{A_6}{A_*} = \frac{A_5}{A_*}\frac{A_6}{A_5}, \quad \text{where } A_* \text{ is the reference area at which } M = 1$$

where

$$\frac{A}{A_*} = \frac{1}{M}\left[\left(\frac{2}{\gamma+1}\right)\left(1+\frac{\gamma-1}{2}M^2\right)\right]^{\frac{\gamma+1}{2(\gamma-1)}} \qquad (7)$$

- between the speed of sound

$$a_6 = a_5 \frac{\sqrt{\left(\frac{T_6}{T_0}\right)}}{\sqrt{\left(\frac{T_5}{T_0}\right)}} \qquad (8)$$

where

$$T = T_0 \,/\, \left(1+\frac{\gamma-1}{2}M^2\right)$$

If the values calculated do not satisfy Equation (6), a new value for $M_5$ ought to be assumed until Equation (6) is satisfied.

In the case of choking conditions in the area contraction, Regions 5 and 6 are connected by the following relationships:

a - Flow downstream the tube

The expansion wave must exist in the narrower part of the tube, which expands the gas from the sonic conditions until $M_6$ and $a_6$ satisfy:

$$Q_4 = Q_6, \text{ i.e.}$$

$$\left(-M_4+\frac{2}{\gamma-1}\right) a_4 = \left(-M_6+\frac{2}{\gamma-1}\right) a_6, \quad \text{where } M_4 = 0,$$

$$P_* = P_6, \text{ i.e.}$$

$$\left(1+\frac{2}{\gamma-1}\right) a_* = \left(M_6+\frac{2}{\gamma-1}\right) a_6, \qquad (9)$$

where $a_*$ is the speed of sound in sonic conditions.

b - Flow upstream the tube

Combining continuity equation between Regions 6 and 5

$$\dot{m} = \rho u A \tag{10}$$

i.e.:

$$\rho_5 u_5 A_5 = \rho_6 u_6 A_6 \quad \text{where } u = Ma \text{ and } M_6 = 1$$

and perfect gas law

$$\rho = \frac{P}{RT} \tag{11}$$

$M_5$ and $a_5$ must satisfy

$$\left(\frac{a_5}{a_6}\right)^{\frac{\gamma+1}{\gamma-1}} = \frac{A_6}{A_5}\frac{M_6}{M_5} \tag{12}$$

and

$$P_3 = P_5$$

$$\left(M_3 + \frac{2}{\gamma-1}\right)a_3 = \left(M_5 + \frac{2}{\gamma-1}\right)a_5 \tag{13}$$

## 2.3 Boundary Conditions

The flow near the open end of the tube cannot be described by simple relationships due to its multidimensional nature. Thus the problem is simplified by assuming quasi one-dimentional, isentropic steady flow.

### 2.3.1 Inflow

For the inflow, the basic energy equation is proposed as a boundary condition

$$p\left(1 + \frac{\gamma-1}{2} M^2\right)^{\frac{\gamma}{\gamma-1}} = p_{0j} \tag{14a}$$

or,

$$\frac{a}{a_j} = \left(\frac{1 + \frac{\gamma-1}{2} M_j^2}{1 + \frac{\gamma-1}{2} M^2}\right)^{1/2} \tag{14b}$$

2.3.2 Outflow

For the outflow two different boundary conditions were used depending on the area ratio of the tube.

(1) For a small area contraction, i.e.: $D_1/D_2 \leq 2$, the constant impulse equation is the boundary condition. Here it is assumed that during outflow, the stream impulse I is constant and equals the stagnation pressure of the jet.

$$I = p + \rho u^2 = p_{0j} \tag{15a}$$

or

$$\frac{a}{a_j} = \left(\frac{p_{0j}/p_j}{1 + \gamma M^2}\right)^{\frac{\gamma-1}{2\gamma}} \tag{15b}$$

(2) For a large area contraction, i.e.: $D_1/D_2 = 4$, the most suitable boundary condition is the assumption of full outflow, i.e.: expansion to the ambient pressure,

$$p = p_j = p_a \tag{16a}$$

or

$$\frac{a}{a_j} = 1 \tag{16b}$$

By applying Equations (14b) and (15b) in the first case or Equations (14b) and (16b) in the second case, one can construct the curve which gives the boundary conditions at

the resonant tube inlet. These relations are shown in Figure 11, for $M_j = 0.6$.

From Figure 11, one can see that during the inflow the maximum value of Mach number cannot exceed 0.6 with $p = p_j$. During the outflow, the Mach number increases according to Equation (15b), for the small area contraction, until a value of 0.443 is reached. For the larger Mach numbers the full outflow is assumed; i.e.: $p = p_j$. (See Figure 11a).

In Figure 11b, it is shown that during the outflow, in the case of the large area contraction, the expansion takes place until the ambient pressure is reached.

The difference between boundary conditions for the outflow can be explained by the difference in the influence of the flow in the smaller tube on the flow in the larger one. The flow in the smaller tube has very little effect on the operation of the large one in the case of large contractions but it cannot be neglected in the case of small area changes.

It ought to be pointed out that the difference between the boundary conditions used for the outflow does not change the values for maximum and minimum pressure obtained in the closed end of the tube. However, stabilization in the wave diagram is reached much faster if the proper boundary conditions are used.

# Chapter 3

## EXPERIMENTAL APPARATUS

The experimental setup consists of a converging nozzle, 10 mm in diameter, with a wire, 0.5 mm in diameter, placed across its exit plane (Figure 12). The diameter of the wire was chosen so that maximum pressure amplitudes could be reached. The availability of tubes of various lengths and diameters simplified the process of construction of the setup. The tubes were placed on a traverse mechanism in order that they could be adjusted concentrically with, and at required separation distance from the nozzle. The latter was mounted on a large plenum chamber with a pressure gage to record the chamber pressure.

At downstream end of the tube, a $p_{cb}$ miniature pressure transducer (sensitive element, 2.5 mm in diameter) was mounted, to record the pressure variations and frequency of oscillations.

For internal flow visualization, a shock tube was used to produce the exciting jet. A schematic of the shock tube and auxilliary equipment is presented in Figure 13. The shock tube consists of two equal length driver and driven sections about 2 m long each. It is square in cross section (50 mm x 50 mm). For flow visualization purposes, at the downstream end of the shock tube, a convergent nozzle, 10 mm in diameter was carefully designed to minimize losses. Mylar

diaphragms, 0.0015 mm thick, were used to yield a shock wave of Mach number 1.29 and an underexpanded sonic jet of stagnation pressure 255 kPa. The resonance tube was carefully placed at the end of the first cell of the exciting jet in order to yield maximum flow oscillations. Various plugs were placed inside the H-S tube to vary its internal shape from the initially square cross sections (10 mm x 10 mm) to the desirable two stepped tube (10 mm, 7 mm and 3.3 mm, each 25 mm long). Commercial glass windows were placed on both sides of the tube to allow flow visualizations.

The optical system used is a conventional spark schlieren system which consists of a 4 KV power supply (with a delay generator to photograph the shock at different instants of time), two parabolic mirrors (1230 mm focal lengths) a knife edge and a camera. Pressure measurements were recorded at the back of the tube, using a $p_{cb}$ piezoelectric pressure transducer. The oscilloscope trace was triggered by means of another transducer placed upstream of the nozzle.

# Chapter 4

# EXPERIMENTAL RESULTS

## 4.1 Flow Visualization in a Stepped Tube

These tests were carried out to visualize both internal flow and shock waves at different phases of the resonant cycle. In these experiments, a square tube with double area contraction was used. The tube's open end was placed axially against the circular nozzle, located at the downstream end of the shock tube's driven section.

A set of spark schlieren photographs are presented in Figure 14. As soon as the flow emanates from the nozzle, inflow starts, thus driving a shock wave into the stepped tube. The interaction of the shock wave with the first and second step is noted in photographs a to d. Due to the area discontinuity, the incident shock will be partially transmitted and partially reflected. The reflection of the transmitted shock from the closed end, and the complex reflected shock flow interaction

is well demonstrated in photograph e. Photographs f and g show the diffracted shock propagating towards the open end; h, i and j demonstrate the outflow phase. In j, the flow emanating from the narrow tube expands to supersonic conditions followed by a standing shock wave. As outflow weakens, an incident shock wave forms near the open end of the tube. The propagation of this shock wave in the middle section of the tube is shown in k, l and m. At the area discontinuity, a transmitted and reflected shock forms and the cycle repeats as before.

From these photographs, it is clear that shock wave propagation in a stepped tube is not a simple one-dimensional plane propagation. The process is complex and it includes shock boundary layer interactions, especially for the reflected shock propagating against the incoming flow. The presence of transmitted and reflected shocks, at the area discontinuity, as well as flow expansion to supersonic values from the samll tube to the intermediate one are also noted.

## 4.2 Pressure Measurement for Variable $D_1/D_2$ Ratio

For pressure measurement the one stepped tube with circular cross section and lengths $L_1$ and $L_2$ of 60 and 50 mm were used. The diameter $D_1$ was chosen equal to 10 mm while the diameter $D_2$ was varied from 2.5 mm to 7.5 mm to give a diameter ratio of 4 to 1.34. Preliminary results show that the pressure amplification increases continuously with the increase in $D_1/D_2$ until little over a diameter ratio of 2. The corresponding length/diameter ratio for the small diameter tube, at this critical point, was found equal to 10. It was therefore concluded that such behaviour could be attributed to the boundary layer. Various tests conducted with shorter tubes for diameter ratio up to 2 were found to give similar results. It was further concluded that the tube length to be used must be less than 10 times the diameter of the tube, otherwise boundary layer could affect the wave amplification due to a sudden area contraction.

Other tests were conducted with tube lengths $L_1$ and $L_2$ equal 25 mm. The diameter of the small tube was varied between 2.5 mm and 7.5 mm. Presure measurements were obtained for different jet Mach numbers, $M_j$ = 0.6, 0.8, 1 and different diameter ratio, $D_1/D_2$, of 4, 2, 1.34 and 1. The values of the pressure from the straight tube were used as a reference for determining the pressure amplitude $\Delta p_R$.

The values obtained experimentally are shown in Table 1.

A typical pressure history at the back of the tube is as shown in Figure 15, for $M_j = 1$; together with the pressure history obtained from a constant area tube. The results for Mach number 0.6, 0.8 and 1 are also shown in Figure 16. From the results one can see that as the diameter ratio $D_1/D_2$ increases, the amplification of the pressure amplitude does not increase monotonically, but asymptotically, approaching a constant value, which in turn depends on the jet Mach number used. The higher the jet Mach number, the lower is the amplification obtained for any given area contraction.

A curve fit was obtained for each Mach number. The pressure amplification was assumed a cubic function of $D_2/D_1$, i.e.:

$$\Delta p_R = A + B(D_2/D_1) + C(D_2/D_1)^2 + E(D_2/D_1)^3$$

and the constants were calculated based on experimental results obtained for each jet Mach number. The following equations were therefore obtained:

$$\Delta p_R = 2.1877 - 2.3652(D_2/D_1) + 3.5307(D_2/D_1)^2 - 2.3532(D_2/D_1)^3 \quad \text{for } M_j = 0.6$$

$$\Delta p_R = 2.0328 - 2.1205(D_2/D_1) + 3.1128(D_2/D_1)^2 - 2.0250(D_2/D_1)^3 \quad \text{for } M_j = 0.8$$

$$\Delta p_R = 1.8782 - 1.8738(D_2/D_1) + 2.6893(D_2/D_1)^2 - 1.6937(D_2/D_1)^3 \quad \text{for } M_j = 1.0$$

It is noted from the three equations that as $D_2/D_1 \to 0$, the pressure amplification reaches the asymptotic values of 2.1877, 2.0328, 1.8782, for $M_j$ of 0.6, 0.8, 1.0, respectively. It should be noted that the asymptotic behaviour of the curves does not mean that the shock is not amplifying with a further decrease in the diameter ratio $D_2/D_1$, because the shock strength is determined based on the pressure ratio across the shock which in turn is dependent on the pressure ahead. The latter, as it will be shown in the next section, is a function decreasing with $D_2/D_1$ and hence this is what limits the pressure behind to the asymptotic value obtained.

# Chapter 5

# THEORETICAL RESULTS

## 5.1 Pressure Amplification for Large Area Contraction

For large area contraction (i.e.: small diameter ratio $D_2/D_1 \to 0$), the fluid dynamic in the small diameter tube can be considered to have little effect on the operation of the larger diameter one, and hence its operation will be similar to that of the constant area tube case. The wave diagram is as shown in Figure 17. It can be seen that regions 1 and 3 give the conditions which control the oscillations in the small diameter tube.

From the method of characteristics and from the assumption that the flow at the contraction behaves like quasi-one dimensional the pressure amplification can be calculated as follows:

### 5.1.1 Regions 2 and 3

$$P_2 = P_*, \text{ i.e.:}$$

$$\frac{a_3}{a_j} = 1 + \frac{\gamma-1}{2} M_j \qquad (17)$$

### 5.1.2 Regions 3 and *

Assuming chocking conditions in region *, which is at the beginning of the narrow part of the tube,

$$M_* = 1, \text{ and}$$

$$a_* = u_* = \frac{a_3}{\sqrt{\frac{1+\gamma}{2}}} \qquad (18)$$

5.1.3 Regions *, 6 and 7

The flow in * undergoes further expansion to supersonic flow. Therefore,

$$P_* = P_6 = P_7, \text{ and}$$

$$\frac{a_7}{a_j} = \sqrt{\frac{\gamma+1}{2}}\left(1 + \frac{\gamma-1}{2} M_j\right) = \frac{a_{max}}{a_j} \qquad (19)$$

5.1.4 Regions 7 and 8

As soon as the compression wave leaves the narrow tube, the flow expands to sonic conditions, i.e.: $M_8 = 1$. Knowing that

$$Q_7 = Q_8, \text{ and } M_7 = 0,$$

the following equation is obtained for the sound spped $a_7$:

$$\frac{a_7}{a_j} = \left(\frac{\gamma-1}{2} + 1\right) \frac{a_8}{a_j} = \frac{a_{max}}{a_j} \qquad (20)$$

5.1.5 Regions 8 and 10

Regions 8 and 10 are related by constant P-wave relationship, i.e.:

$$P_8 = P_{10}, \text{ and}$$

$$\frac{a_{10}}{a_j} = \left(1 - \frac{\gamma-1}{2}\right) \frac{a_8}{a_j} \qquad (21)$$

Combining (19), (20) and (21), the following relation is obtained for the minimum value of the speed sound, $a_{10}$

$$\frac{a_{min}}{a_j} = \frac{3-\gamma}{\sqrt{2(1+\gamma)}}\left(\frac{\gamma-1}{2} M_j + 1\right) = \frac{a_{10}}{a_j} \qquad (22)$$

So the pressure amplitude is

$$\frac{\Delta p}{p_j} = \left(\frac{a_7}{a_j}\right)^{\frac{2\gamma}{\gamma-1}} - \left(\frac{a_{10}}{a_j}\right)^{\frac{2\gamma}{\gamma-1}} \qquad (23)$$

and,

$$\frac{\Delta p}{p_j} = \left(\frac{\gamma-1}{2} M_j + 1\right)^{\frac{2\gamma}{\gamma-1}} \left\{\left(\frac{\gamma+1}{2}\right)^{\frac{\gamma}{\gamma-1}} - \left(\frac{3-\gamma}{2(1+\gamma)}\right)\right\}^{\frac{2\gamma}{\gamma-1}} \qquad (24)$$

Taking the ratio, between $\Delta p$ for the stepped tube and that for the simple one, the following equation is obtained for $\Delta p_R$

$$\Delta p_R = \frac{\left(\frac{\gamma+1}{2}\right)^{\frac{\gamma}{\gamma-1}} - \left(\frac{3-\gamma}{\sqrt{2(1+\gamma)}}\right)^{\frac{2}{\gamma-1}}}{1 - \left(\frac{1 - \frac{\gamma-1}{2} M_j}{1 + \frac{\gamma-1}{2} M_j}\right)^{\frac{2\gamma}{\gamma-1}}} \qquad (25)$$

For $\gamma = 1.4$,

$$\Delta p_R = \frac{1.78214}{\left[1 - \left(\frac{1 - 0.2\, M_j}{1 + 0.2\, M_j}\right)^7\right]} \qquad (26)$$

This relationship is plotted in Figure 18 as a function of jet Mach number. Good agreement is noted between theory and experiments for this limiting case of large area contraction.

The assumption of choking conditions in the area contraction is valid only for jet Mach number $M_j > 0.215$, which provides such pressure gradient that the gas is accelerated to supersonic flow. For $M_j < 0.215$, the flow between

regions 2 and 6 remains subsonic and detailed solution for this case must be iterated for each $M_j$.

## 5.2 Pressure amplification for Small Area Contraction

The values of Riemman invariants P and Q for the waves propagating through the area contraction are changed and, for small area contraction, these changes can be described based on the following equations [13]:

$$\Delta^+ P = -\frac{ua}{u+a}\Delta^+ \ln A$$
$$\Delta^- Q = -\frac{ua}{u-a}\Delta^- \ln A \qquad (27)$$

where $\Delta^\pm \ln A = \pm \ln \frac{A_2}{A_1}$

The wave diagrams were constructed as shown in Figure 19.

$P_2 = P_3 = P_1 + \Delta^+ P$ i.e.:

$$\frac{a_3}{a_j} = \left(\frac{\gamma-1}{2} M_j + 1\right) - \left(\frac{\gamma-1}{2}\frac{M_j}{M_j+1} \ln \frac{A_2}{A_1}\right) = \frac{a_{max}}{a_j}, \text{ where } M_3 = 0 \qquad (28)$$

$P_5 = P_6 = P_4 + \Delta^+ P$ i.e.:

$$\frac{a_6}{a_j} = \left(\frac{\gamma-1}{2} M_j + 1\right) - \left(\frac{\gamma-1}{2}\frac{M_j}{M_j-1} \ln \frac{A_2}{A_1}\right) = \frac{a_{min}}{a_j}, \text{ where } M_6 = 0 \qquad (29)$$

The pressure amplitude can be described as,

$$\frac{\Delta p}{p_j} = \left(\frac{a_3}{a_j}\right)^{\frac{2\gamma}{\gamma-1}} - \left(\frac{a_6}{a_j}\right)^{\frac{2\gamma}{\gamma-1}} \qquad (30)$$

with $D_1/D_2 \to 1$, the above equation can be expanded to yield the following approximate relation:

$$\frac{\Delta p}{p_j} = 2\gamma M_j\left(1 + 2 \ln \frac{D_1}{D_2} \frac{1 - \frac{\gamma+1}{2} M_j^2}{1 - M_j^2}\right) \tag{31}$$

For small area contraction, after expansion in power series

$$\ln \frac{D_1}{D_2} \approx 2 \frac{(1 - \frac{D_2}{D_1})}{(1 + \frac{D_2}{D_1})}$$

and the pressure amplitude ratio is

$$\Delta p_R = \left[1 + 4 \frac{(1 - \frac{D_2}{D_1})}{(1 + \frac{D_2}{D_1})} - \frac{(1 - \frac{\gamma+1}{2} M_j^2)}{(1 - M_j^2)}\right] \tag{32}$$

for $\gamma = 1.4$, Equation (32) becomes,

$$\Delta p_R = \left[1 + 4 \frac{(1 - \frac{D_2}{D_1})}{(1 + \frac{D_2}{D_1})} \frac{(1 - 1.2\ M_j^2)}{(1 - M_j^2)}\right] \tag{33}$$

The results are presented in Figure 20 for jet Mach numbers 0.6 and 0.8. As noted in Figure 20, the calculated values agree well with the experimental ones for small area reduction. For area change greater than 1.69, a more detailed analysis is required to include both the transmitted and the reflected waves at the area discontinuity section. This case will be presented in the following section.

## 5.3 Detailed Wave Diagram for $M_j = 0.6$ and Diameter Ratios of 1.34, 2 and 4

For diameter ratios of 1.34, 2 and 4, detailed wave diagrams were constructed. Each wave interaction with the area discontinuity results in a transmitted wave and a reflected wave. This complicated case was, however, simplified by constructing the wave diagram with each family of wave having constant slope; thus eliminating the extra work which could result from drawing wave diagram with actual slopes.

A typical wave diagram is shown in Figure 21 for $M_j = 0.6$ and diameter ratio of 1.34. In Figure 21 some of the values of flow Mach number and sound speed are shown together with the flow directions. From these values both the amplitude and the frequency of oscillations were calculated. The same procedure was carried out for the other area contraction ratios. However, for the diameter ratio 4, which can be treated as a large area contraction, the pressure amplitude was calculated in two different ways, depending on assumptions.

### 5.3.1 Case 1

The flow in each part of the tube affects the flow in another one, i.e.: there is an isentropic flow between two parts of the stepped tube in both directions (the case described above in Chapter 2).

5.3.2 Case 2

The flow in the small diameter tube is affected by inflow from the larger tube, but outflow is so small that it can be neglected; i.e.: there is an isentropic flow between two parts of the stepped tube only in one direction. There is no isentropic outflow from the narrower part of the tube.

Table 2 and Figure 22 show the results, i.e.: the pressure amplitude as a function of the diameter ratio, where for $D_1/D_2 = 4$, the two cases are included.

Comparing the theoretical results with experimental ones, it can be seen that probably the most adequate $\Delta p_R$ value for the diameter ratio $D_1/D_2 = 4$, would be obtained by taking the average between two values from cases 1 and 2. However, not to complicate calculations further it was decided to take Case 1, as adequate to describe flow for the tube with diameter ratio $D_1/D_2 \leq 4$, and to use Case 2 for each large but finite diameter ratio, $D_1/D_2 > 4$.

All above calculations were obtained assuming the length ratio of the two parts of the tube $L_1/L_2 = 1$.

In addition to this, some calculations were made using other length ratios, such as $L_1/L_2 = 0.75$ and 1.25. The results presented in Table 3 and Figure 23 show that there is not a meaningful difference; however, the pressure amplitude obtained for the length ratio different from 1 is slightly higher (but less than 5%).

Because the calculations are more time consuming and more complicated, further investigations were limited only to the length ratio $L_1/L_2 = 1$ case.

One of the wave diagram, for $M_j = 0.6$, $D_1/D_2 = 4$ and $L_1/L_2 = 1.25$, together with the pressure history in the closed end and the flow direction, is shown in Figure 24.

In Table 4, some of the values of flow Mach number and sound speed are presented.

This diagram can be compared with the wave diagram in Figure 25, for the tube of length ratio $L_1/L_2 = 1$ and same diameter ratio $D_1/D_2 = 4$. Some values of the flow Mach number and sound speed are presented in Table 5.

From both figures it can be seen that length ratio different from 1 much more complicates the wave diagram, but that it does not change significantly the value of the pressure amplitude.

# Chapter 6

## FREQUENCY OF OSCILLATIONS

### 6.1 Frequency of Oscillation for the Simple H-S Tube

The frequency of the simple H-S tube was chosen as a reference state for that of the stepped tube. The calculations were obtained as follows (Figure 26):

Knowing the velocity of the air coming in and out of the tube and the speed of the sound before and after the reflection from the closed end, the average velocity of the waves can be calculated as:

$$V_{12} = \frac{(1 + M_j)\, a_j + a_{min}}{2} = V_{45}$$

$$V_{23} = \frac{(1 - M_j)\, a_j + a_{max}}{2} = V_{34}$$

where $a_{max} = (1 + \frac{\gamma-1}{2} M_j)\, a_j$ and

$a_{min} = (1 - \frac{\gamma-1}{2} M_j)\, a_j$ so,

$$V_{12} = V_{45} = \left[1 + (\tfrac{3-\gamma}{4})\, M_j\right] a_j \qquad (34)$$

$$V_{23} = V_{34} = \left[1 - (\tfrac{3-\gamma}{4})\, M_j\right] a_j \qquad (35)$$

The time required for the waves to go through the tube until the cycle is repeated is

$$t_p = L_s \left(\frac{1}{V_{12}} + \frac{1}{V_{23}} + \frac{1}{V_{34}} + \frac{1}{V_{45}}\right),$$

where $L_s = L_1 + L_2 = 2 L_1 = 2 L_2$

so $$t_p = \frac{4 L_s}{\left[1 - \left(\frac{3-\gamma}{4}\right)^2 M_j^2\right] a_j} = \frac{8 L_2}{\left[1 - \left(\frac{3-\gamma}{4}\right)^2 M_j^2\right] a_j}$$

and the frequency of oscillation is

$$f_s = \frac{1}{t_p} = \frac{\left[1 - \left(\frac{3-\gamma}{4}\right)^2 M_j^2\right] a_j}{8 L_2} \qquad (36)$$

for the $\gamma = 1.4$

$$f_s = \frac{(1 - 0.16 M_j^2)\, a_j}{8 L_2} \qquad (37)$$

Table 6 and Figure 27 show how nondimensional frequency of oscillations, $f_s/f_0$, for the simple H-S tube depends on the Mach number of the jet which drives the tube. Its value monotically decreases with increasing jet Mach number. The theoretical results agree well with those obtained experimentally for the simple tube of L = 0.127 m.

## 6.2 Frequency of Oscillations for the Stepped Tube and Different Diameter Ratios

For each wave diagram obtained, based on theoretical analysis, the frequency of oscillations was calculated. The velocity of the waves was taken as an average of absolute velocities of the flow in front and behind the wave. According to Figure 28,

$$V_{12} = \frac{u_1 + a_1}{2} + \frac{u_2 + a_2}{2} = \frac{a_1 + a_2\ (1 + M_2)}{2}$$

$$V_{23} = \frac{-u_2 + a_2}{2} + \frac{u_3 + a_3}{2} = \frac{a_3 + a_2\ (1 - M_2)}{2}$$

and

$$t_1 = L_2\ (\frac{1}{V_{12}} + \frac{1}{V_{34}})$$

$$V_{34} = \frac{u_3 + a_3}{2} + \frac{-u_4 + a_4}{2} = \frac{a_3 + a_4\ (1 - M_4)}{2}$$

$$V_{45} = \frac{u_4 + a_4}{2} + \frac{u_5 + a_5}{2} = \frac{a_5 + a_4\ (1 + M_4)}{2}$$

and

$$t_2 = L_2\ (\frac{1}{V_{34}} + \frac{1}{V_{45}})$$

the period of the cycle is

$$t_p = t_1 + t_2$$

and the frequency of oscillations

$$f = \frac{1}{t_p}$$

$$f = \frac{a_j}{2L_2}\left[\frac{1}{\frac{a_j}{a_1+a_2(1+M_2)}+\frac{a_j}{a_3+a_2(1-M_2)}+\frac{a_j}{a_3+a_4(1+M_4)}+\frac{a_j}{a_5+a_4(1-M_4)}}\right]$$

The frequency of the simple tube was used as the state of reference.

During the experiments the frequency of oscillations was recorded for different jet Mach number and area ratio. The comparison of the experimental and theoretical results is presented in Table 7 and Figure 29.

In Figure 29 it is seen that the frequency of oscillations is found to vary with the diameter ratio: the higher the diameter ratio, the higher the frequency of oscillations. The same results were obtained from the detailed pressure measurement at the downstream end of the small tube.

## 6.3 Frequency of Oscillations for the Large Area Contraction ($D_1/D_2 \to \infty$)

In the case of the large area contraction, two parts of the tube can be treated as two independent tubes (Figure 30).

Knowing,

$$a_{max} = \sqrt{\frac{\gamma+1}{2}}\left(\frac{\gamma-1}{2}M_j + 1\right) a_j \qquad (39)$$

and,

$$a_{min} = \frac{3-\gamma}{\gamma+1}\sqrt{\frac{\gamma+1}{2}}\left(\frac{\gamma-1}{2}M_j + 1\right) a_j \qquad (40)$$

and assuming sonic conditions in the area contraction, i.e.:

$$M_* = \pm 1,$$

the speed of sound is,

$$a_* = \frac{a_{min}}{(\frac{\gamma-1}{2} M_* - 1)} = \frac{a_{max}}{(\frac{\gamma-1}{2} M_* + 1)} = \sqrt{\frac{2}{\gamma+1}} \, (\frac{\gamma-1}{2} M_j + 1) \, a_j$$

The average speed of the waves is,

$$V_{12} = V_{45} = \frac{a_* \, (M_* + 1) + a_{min}}{2} = a_* + \frac{a_{min}}{2}$$

$$V_{23} = V_{34} = \frac{a_* \, (M_* - 1) + a_{max}}{2} = \frac{a_{max}}{2}$$

and the period,

$$t_p = t_1 + t_2 = L_2 \, (\frac{2}{V_{12}} + \frac{2}{V_{23}})$$

The frequency of oscillation for $D_1/D_2 \to \infty$, $f = \frac{1}{T}$ is equal to

$$f = \frac{a_j}{4L_2} \left\{ \frac{1}{\frac{1}{(\frac{\gamma-1}{2} M_j+1)\left[\sqrt{\frac{8}{\gamma+1}} + (3-\gamma)\sqrt{\frac{1}{2(\gamma+1)}}\right]} + \frac{1}{\sqrt{\frac{\gamma+1}{2}} \, (\frac{\gamma-1}{2} M_j+1)}} \right\} \tag{41}$$

what for $\gamma = 1.4$ gives

$$f = 0.1917 \, (0.2 \, M_j + 1) \, \frac{a_j}{L_2} \tag{42}$$

and

$$f / f_s = 1.5336 \left(\frac{1 + 0.2\ M_j}{1 - 0.16\ M_j^2}\right) \qquad (43)$$

In Table 8 and Figure 31 is shown the relation between frequency of oscillation and driving jet Mach number for $D_1/D_2 \to \infty$.

The results presented here show that frequency amplification $f / f_s$ increases with increasing jet Mach number for large area contraction.

# Chapter 7

## SUMMARY AND CONCLUSIONS

A detailed theoretical analysis to the internal flow in an H-S tube with a sudden area contraction has been presented. The above analysis includes solutions to the two limiting cases of large and small area changes. Solution to the intermediate area change has also been presented. The experimental results obtained from pressure measurements and spark schlieren photography are found to be in close correlation with those obtained theoretically. The main conclusions to be drawn from this work are that,

1 - The internal flow dynamics in a stepped H-S tube can be successfully analysed by considering the sudden area change as a discontinuity and by the use of the method of characteristics. The pressures on both sides of discontinuity are not equal and therefore the CCW A-M relationship cannot be used as in the past [10], in detailing both shock and pressure amplifications.

2 - The pressure amplitude increases with the increase in diameter ratio, $D_2/D_1$. The increase approaches a constant value which depends on the jet Mach number used.

3 - The percentage increase in the pressure amplitudes, as compared to constant area values, is found to decrease with the increase in the jet Mach number.

4 - The pressure amplitude $\Delta p_R$ can be described for two limiting cases by formulas

a) for large area contraction, $D_1/D_2 \to \infty$

$$\Delta p_R = \frac{1.78214}{1 - \left(\frac{1 - 0.2\ M_j}{1 + 0.2\ M_j}\right)} \quad \text{for } \gamma = 1.4 \text{ and } M_j > 0.215$$

b) for small area contraction, $D_1/D_2 \leq 1.3$

$$\Delta p_R = \left[1 + 4\ \frac{(1 - D_2/D_1)}{(1 + D_2/D_1)}\ \frac{(1 - 1.2\ M_j^2)}{(1 - M_j^2)}\right] \quad \text{for } \gamma = 1.4 \text{ and } M_j \leq 0.8$$

5 - For different length ratios in two sections of a stepped H-S tube, no significant changes were noted in the pressure amplitude. The variation is found to be less than 5%.

6 - The frequency of oscillation for the simple H-S tube decreases with increasing jet Mach number $M_j$. It can be described by formula

$$f_s = \frac{(1 - 0.16\ M_j^2)\ a_j}{4\ L_s} \quad \text{for } \gamma = 1.4$$

7 - The frequency of oscillation for the stepped H-S tube increases with the area ratio. For large area contractions, the frequency of oscillation approaches that corresponding to the upstream portion of the stepped tube.

8 - The frequency of oscillations for the large area contraction, $D_1/D_2 \to \infty$, is found to increase with increasing jet Mach number.

$$f / f_s = 1.5336 \frac{(1 + 0.2\ M_j)}{(1 - 0.16\ M_j^2)} \quad \text{for } \gamma = 1.4$$

Although the present theoretical work was for an H-S tube with one area contraction, excited by subsonic jets, the computational and analytical methods presented here could be applied to more generalized cases in the future.

## REFERENCES

1. Hartmann, J., and Troll, B., "On a New Method for the Generation of Sound Waves," Phys. Rev., 20, 1922, pp 719-727.

2. Sprenger, H.S., "Uber Thermische Effekte bei Rezonanzrohren," Mitteileungen aus dem Institut für Aerodynamik an der E.T.H., Zürich, Nr. 21, 1954, pp 18-35.

3. Hartmann, J., "Production by Means of an Air-Jet of Acoustic Waves of Velocity Exceeding that of Sound," Phil. Mag., Vol. 11, April 1931, pp 926-948.

4. Stabinsky, I. et al, "Space Shuttle Auxiliary Propulsion Ignitor System," System Quarterly Technical Progress Narratives under Contract NAS3-14351, August 1970 to January 1971, Reports No.'s ASR 70-460, ASR 71-45.

5. Rakowsky, E.L. and Corrado, A.P., "An Experimental Investigation of a Flueric Explosive Ignition Device (U)," 6th Symposium on Electro-explosive Devices (EED's), Franklin Institute Research Labs, San Francisco, CA, July 8-10, 1969.

6. Rakowsky, E.L., Corrado, A.P. and Marchesse, V.P., "Fluid Explosive Initiator," Sixth Cranfield Fluidics Conference, paper H4, 26th-28th March 1974, Cambridge, pp 29-42.

7. Neemeh, R.A., Ostrowski, P.P. and Wu, J.H.T., "Thermal Performance of a Logarithmic-Spiral Resonance Tube," AIAA Journal, Vol. 22, No. 12, 1984, pp 1823-1825.

8. Wu, J.H.T., Ostrowski, P.P., Neemeh, R.A. and Lee, P.H.W., "Experimental Investigation of a Cylindrical Resonator," AIAA Journal, Vol. 12, August 1974, pp 1076-1078.

9. Neemeh, R.A. et al, "Cylindrical Resonators," Proceedings of the 13th International Symposium on Shock Tubes and Waves, Niagara Falls, July 6-9, 1981, pp 385-391.

10. Brocher, E., "Amplification of Non-linear Standing Waves in a Cylindrical Cavity with Varying Cross Section," Proceedings of the 13th International Symposium on Shock Waves and Shock Tubes, State University of New York Press, Albany, N.Y., 1981, p 209.

11. Brocher, E. and Kawahashi, M., "Wave and Thermal Phenomena in H-S Tubes with an Area Constriction," Proceedings of the 15th International Symposium on Shock Waves and

Shock Tubes, Stanford University Press, Berkeley, CA, July 28-August 2, 1985, pp 179-185.

12. Wu, J.H.T., Neemeh, R.A. and Ostrowski, P.P., "Subsonic Jet Driven Resonance Tube," C.A.S.I. Transactions Vol. 8, No. 1, March 1975.

13. Rudinger, G., "Nonsteady Duct Flow Wave - Diagram Analysis," D. Van Nostrand Company Inc., New York, N.Y., 1955.

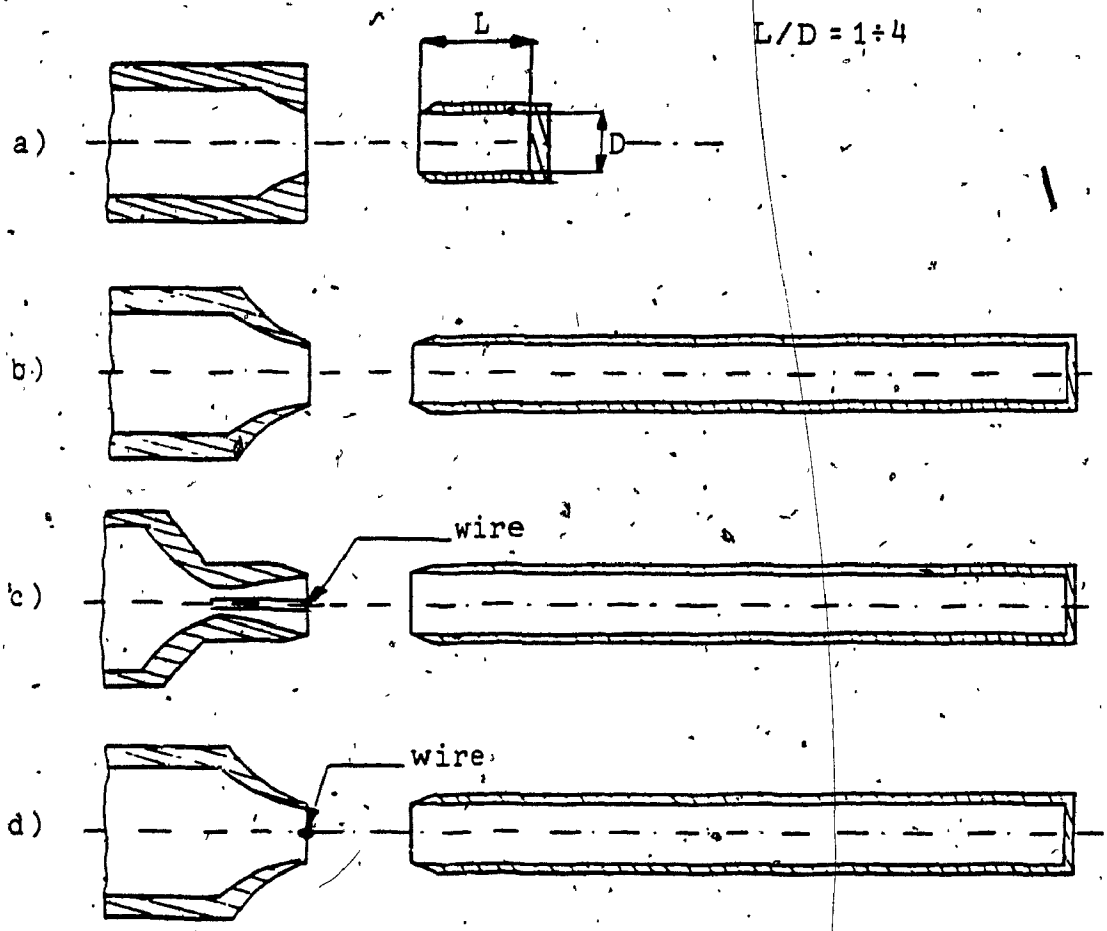


Figure 1. The resonance tubes

a) Hartmann's oscillator
b) Simple tube - periodic jet
c) Simple tube - supersonic jet
d) Simple tube - subsonic jet

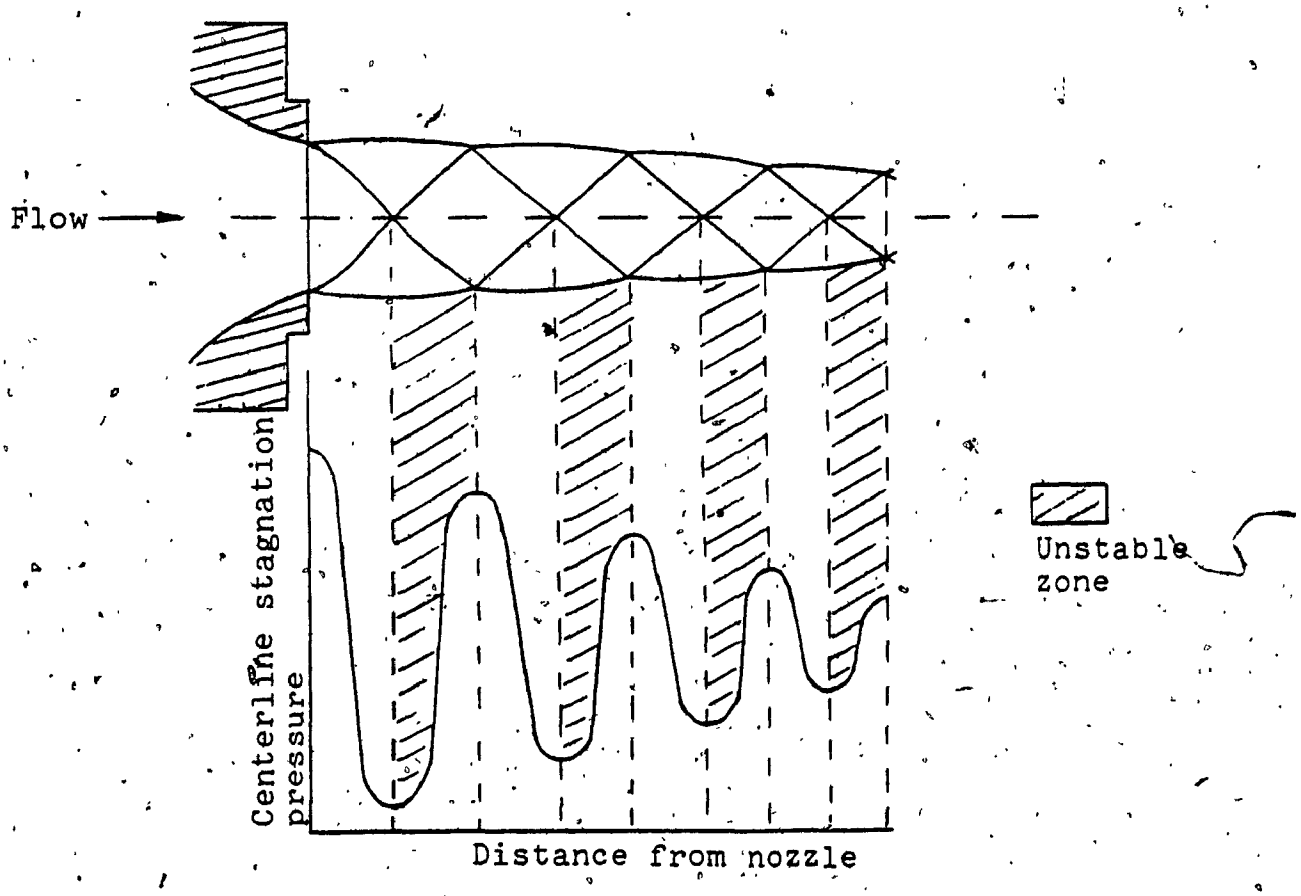


Figure 2. Typical variation of stagnation pressure in an underexpanded periodic jet

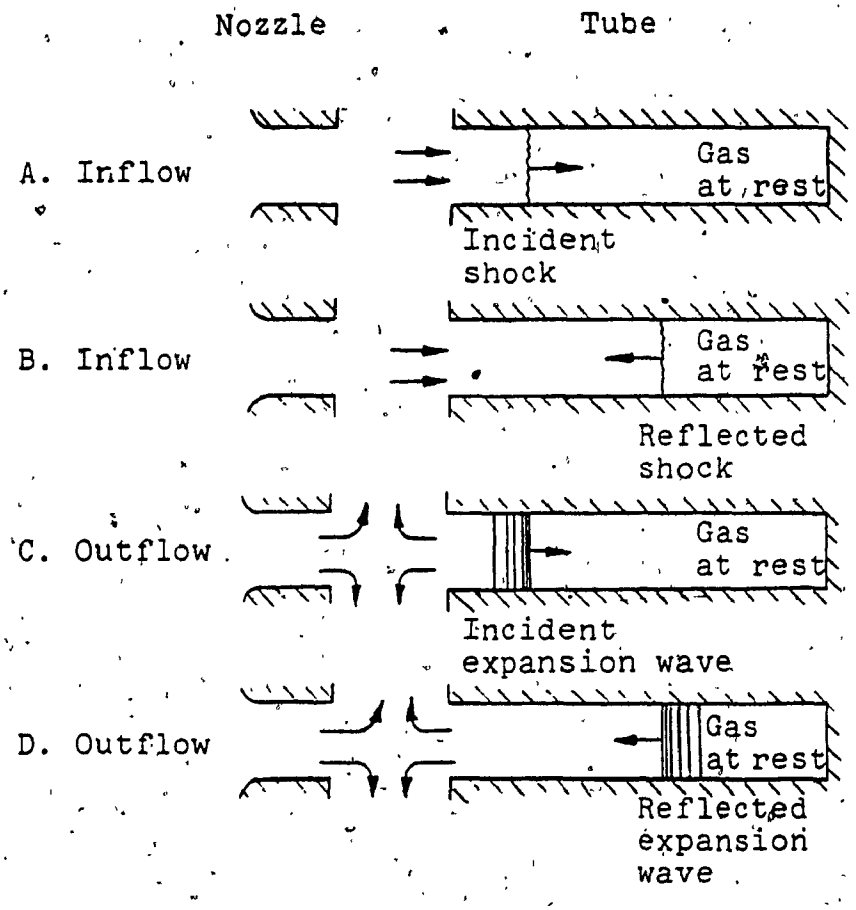


Figure 3. The resonant cycle within the simple H-S tube

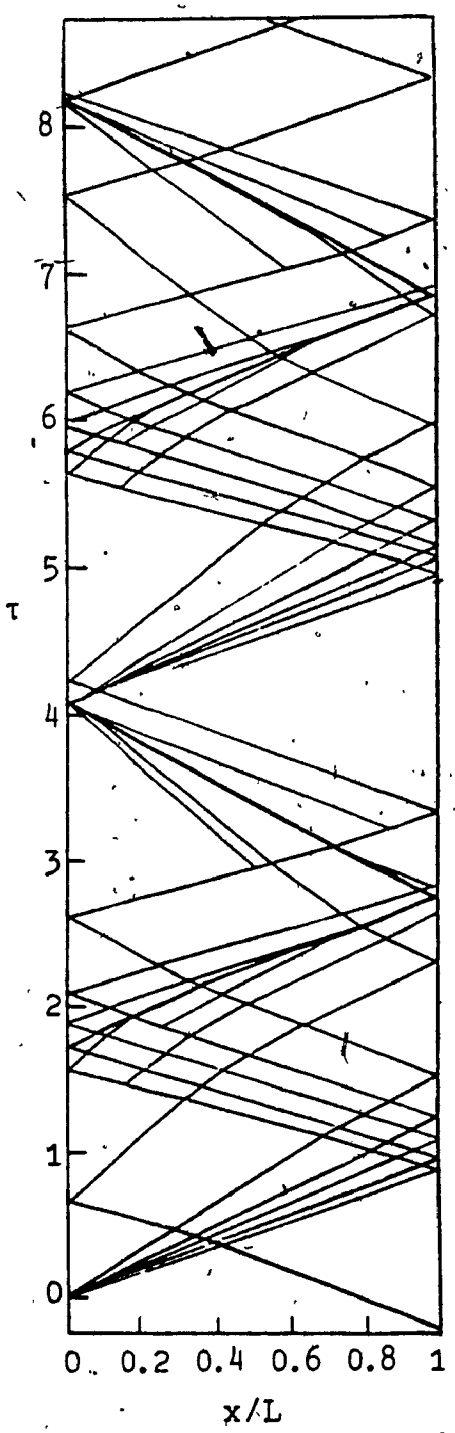


Figure 4. Detailed wave diagram for the simple tube

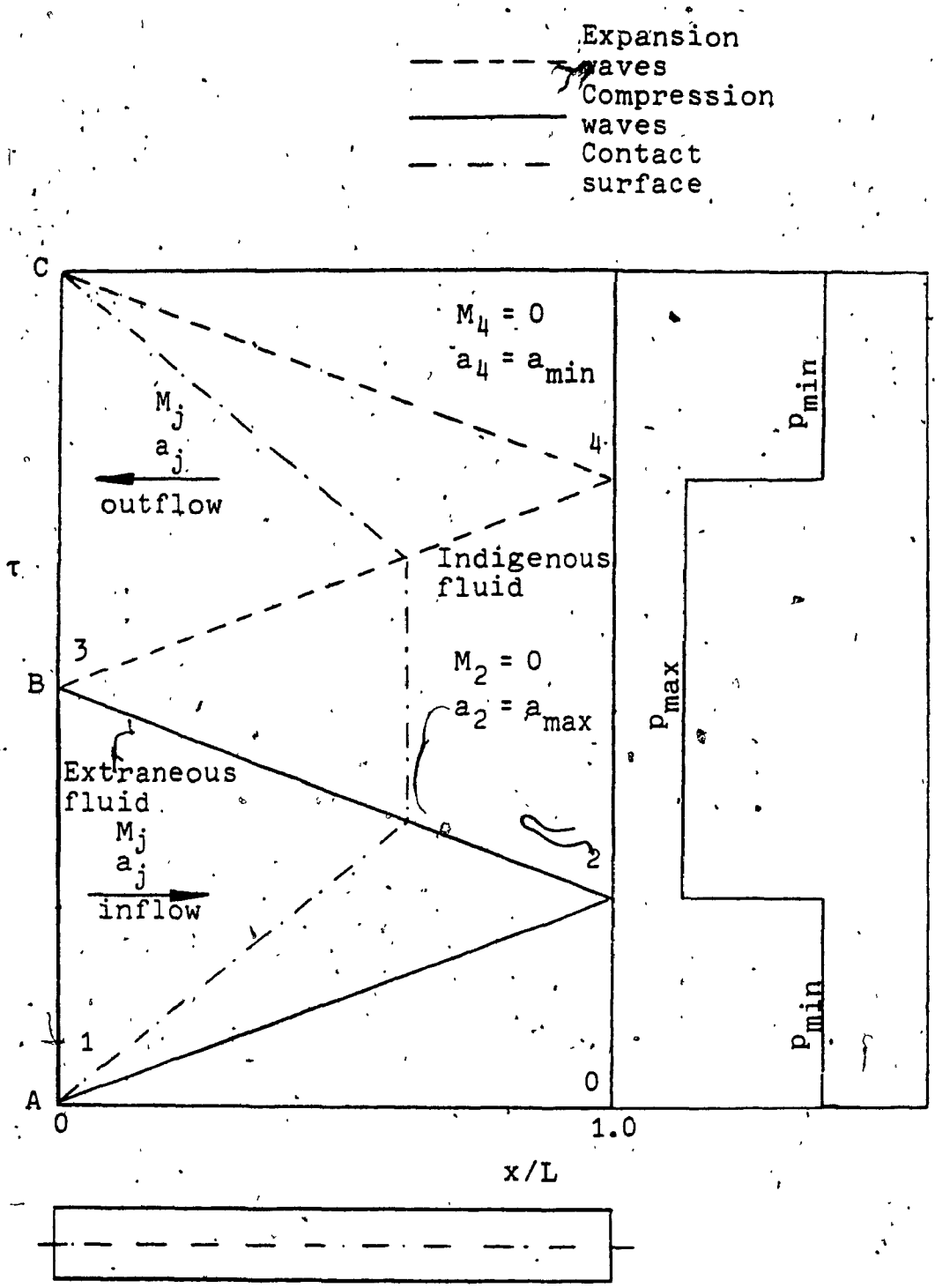


**Figure 5.** Simplified wave diagram for the simple tube

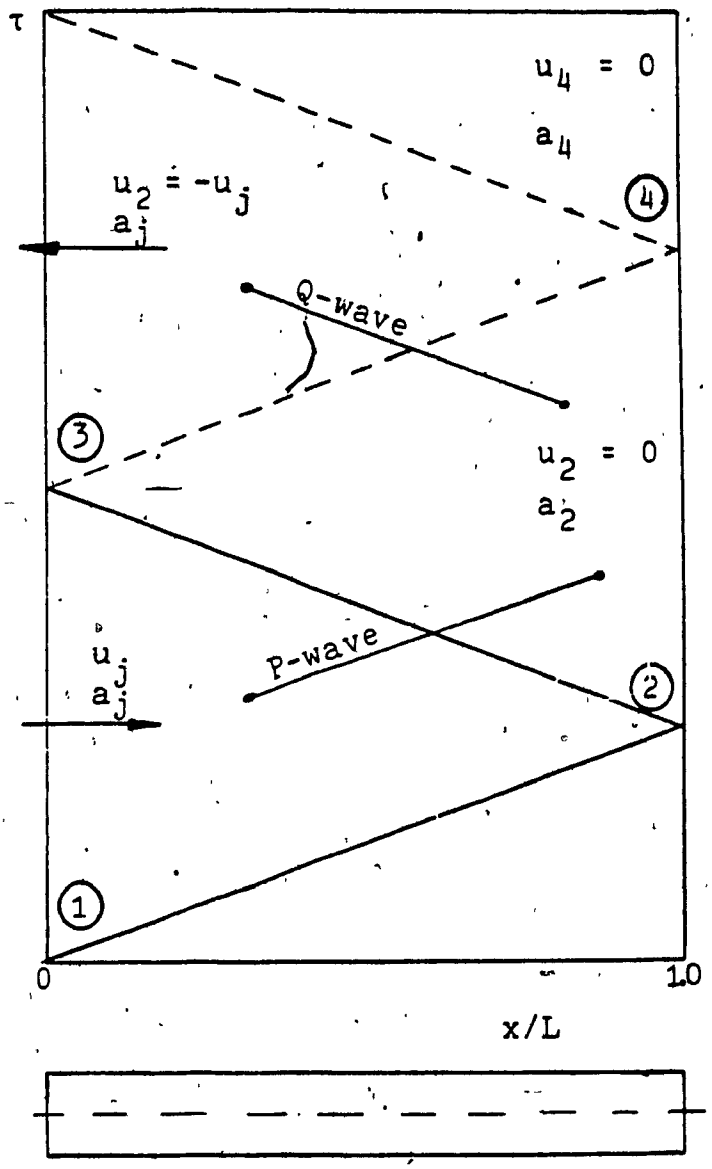


Figure 6. Wave diagram for method of characteristics (simple tube)

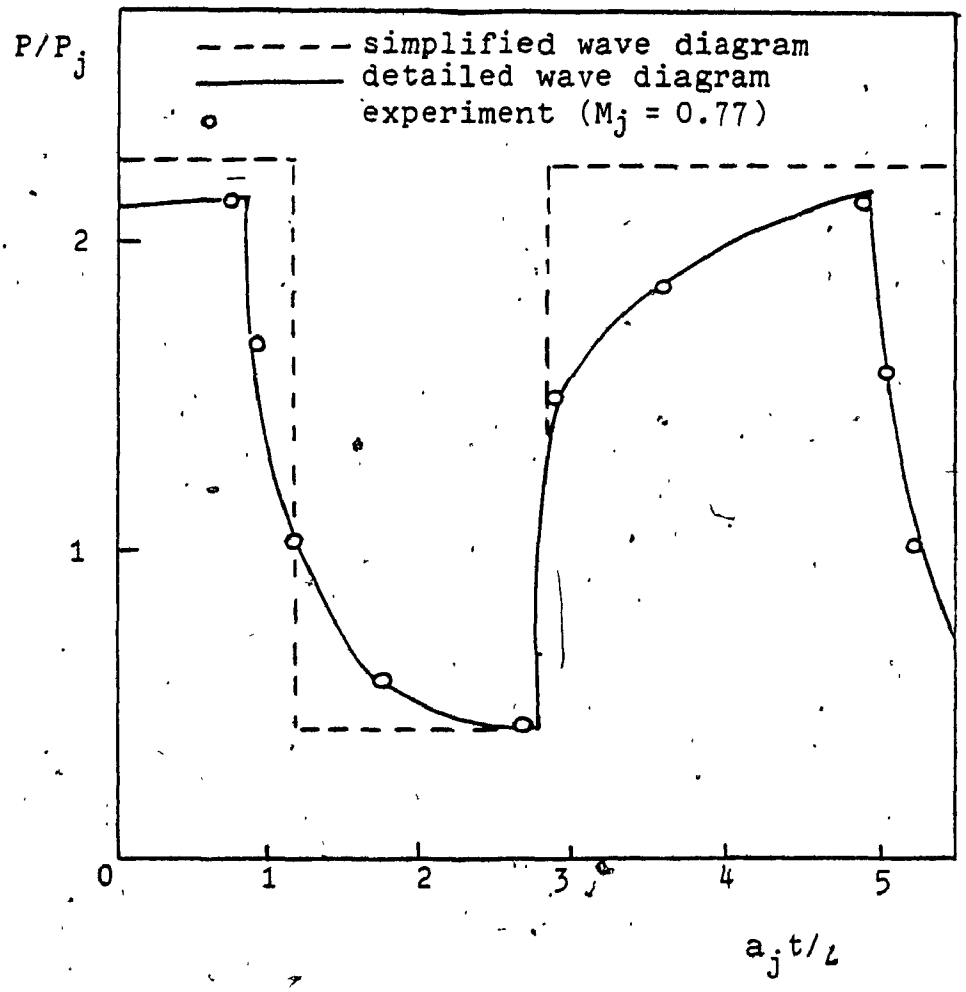


Figure 7. The pressure history at the closed end of the resonance tube

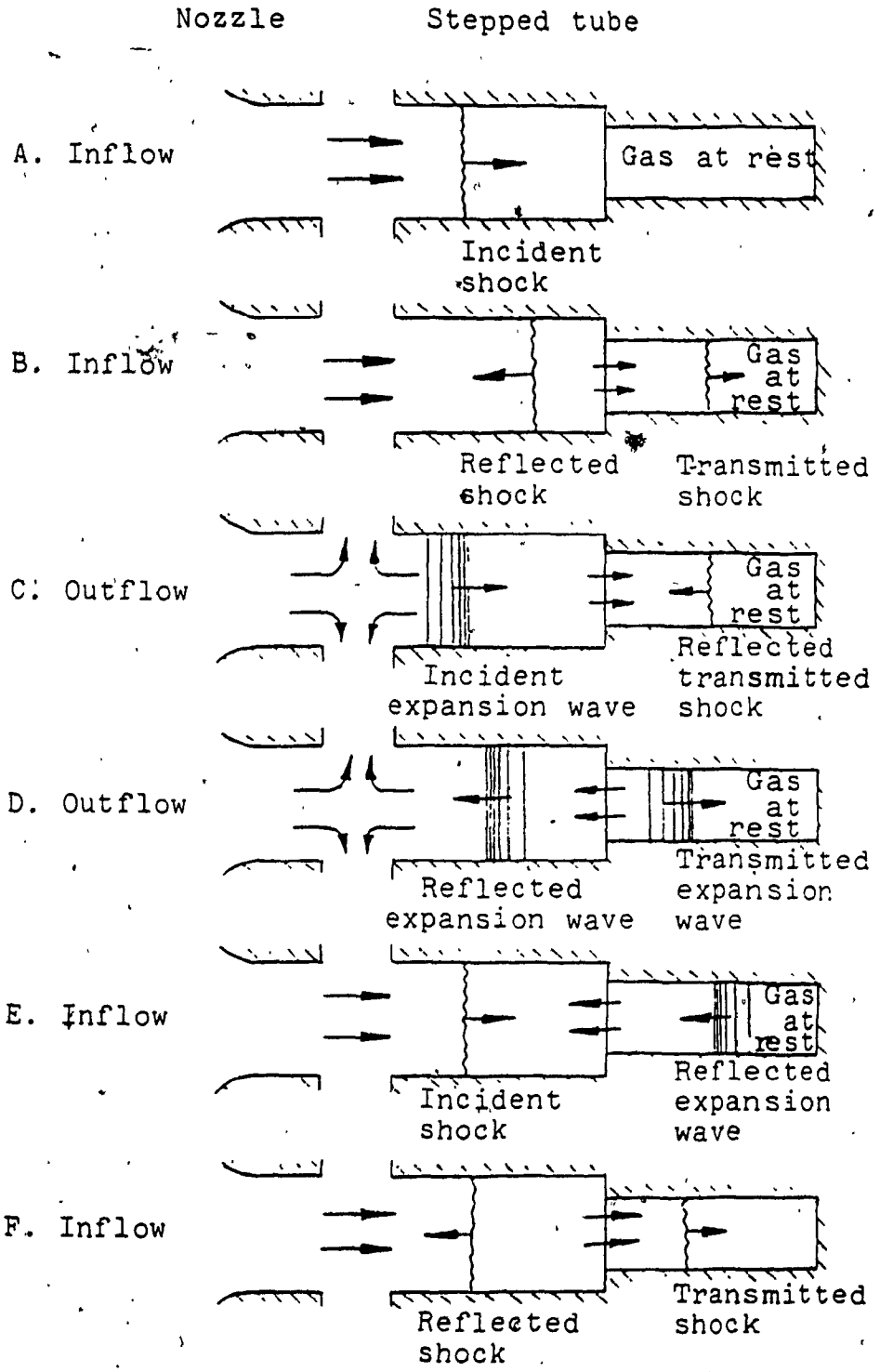


Figure 8. The resonance cycle within the stepped H-S tube

——— Shock wave
------ expansion wave
I.S.W. incident shock wave
T.S.W. transmitted shock wave
R.S.W. reflected shock wave

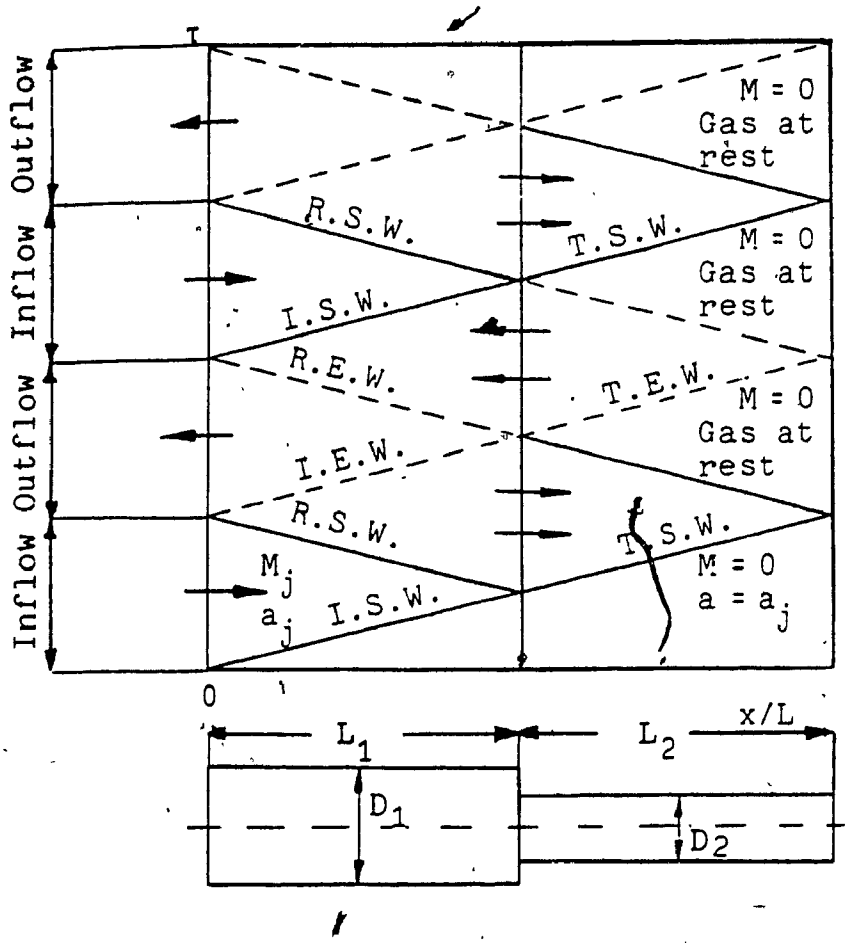


Figure 9. Simplified wave diagram for the stepped tube

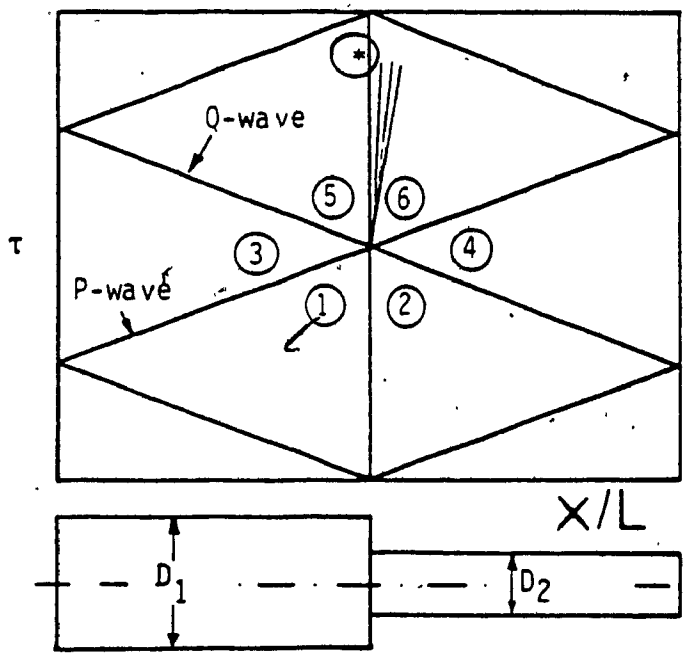


Figure 10. Wave diagram in the junction for the stepped tube

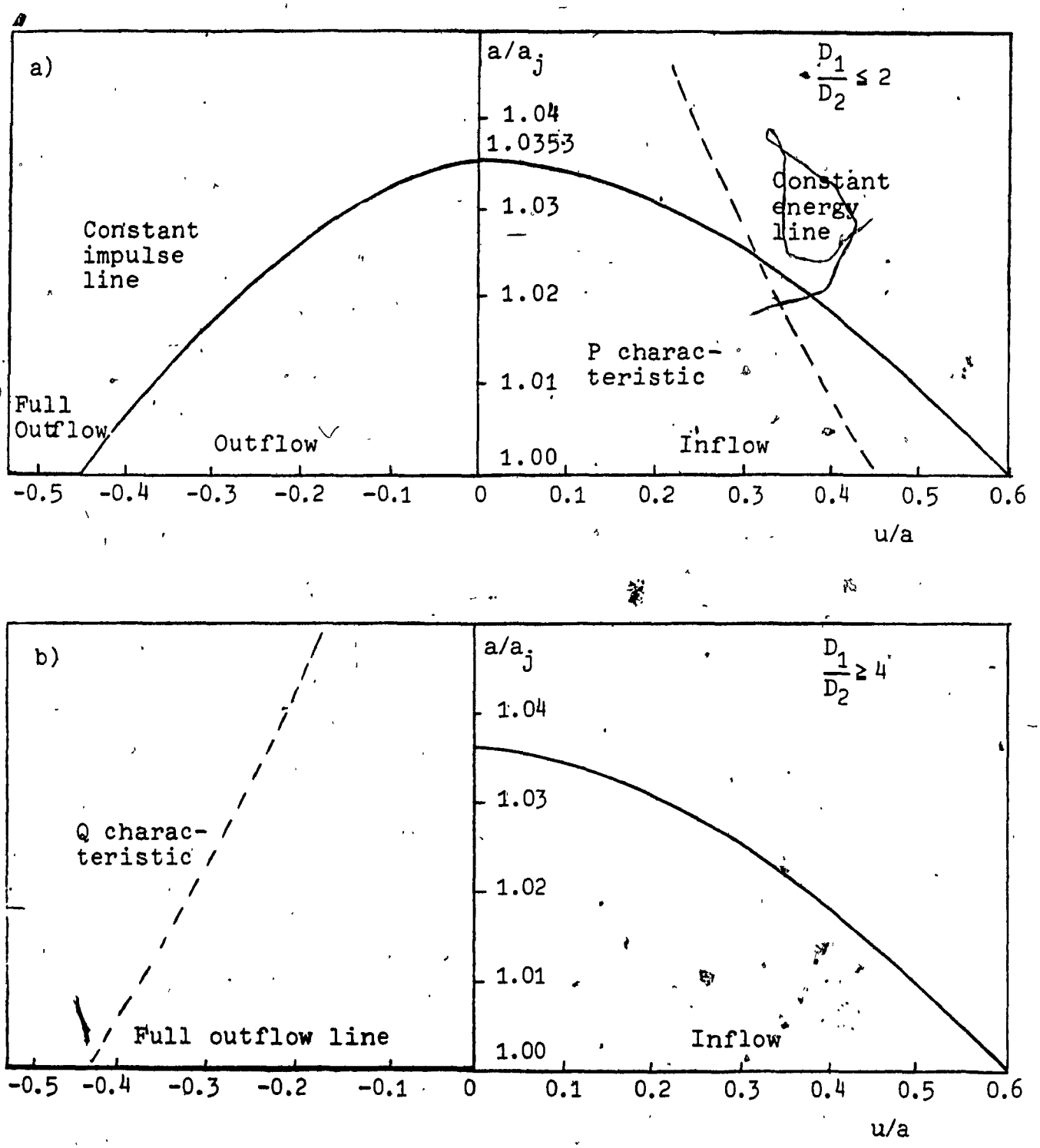


Figure 11. Boundary conditions for inflow and outflow from resonance tube for the subsonic jet
a) for diameter ratio $D_1/D_2 \leq 2$
b) for diameter ratio $D_1/D_2 \geq 4$

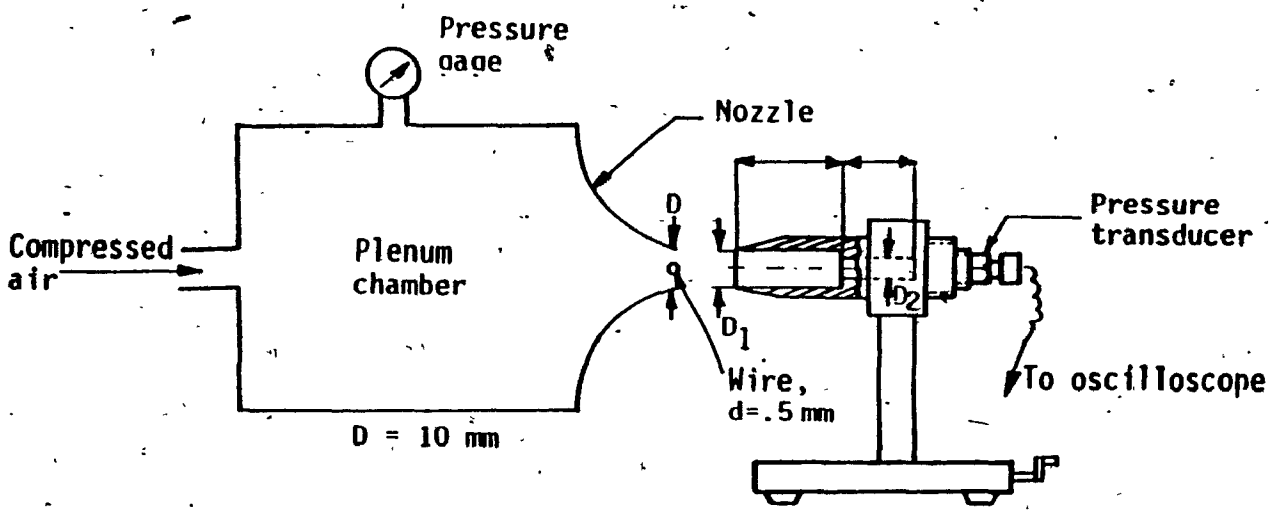


Figure 12. Experimental apparatus and tube with area contraction

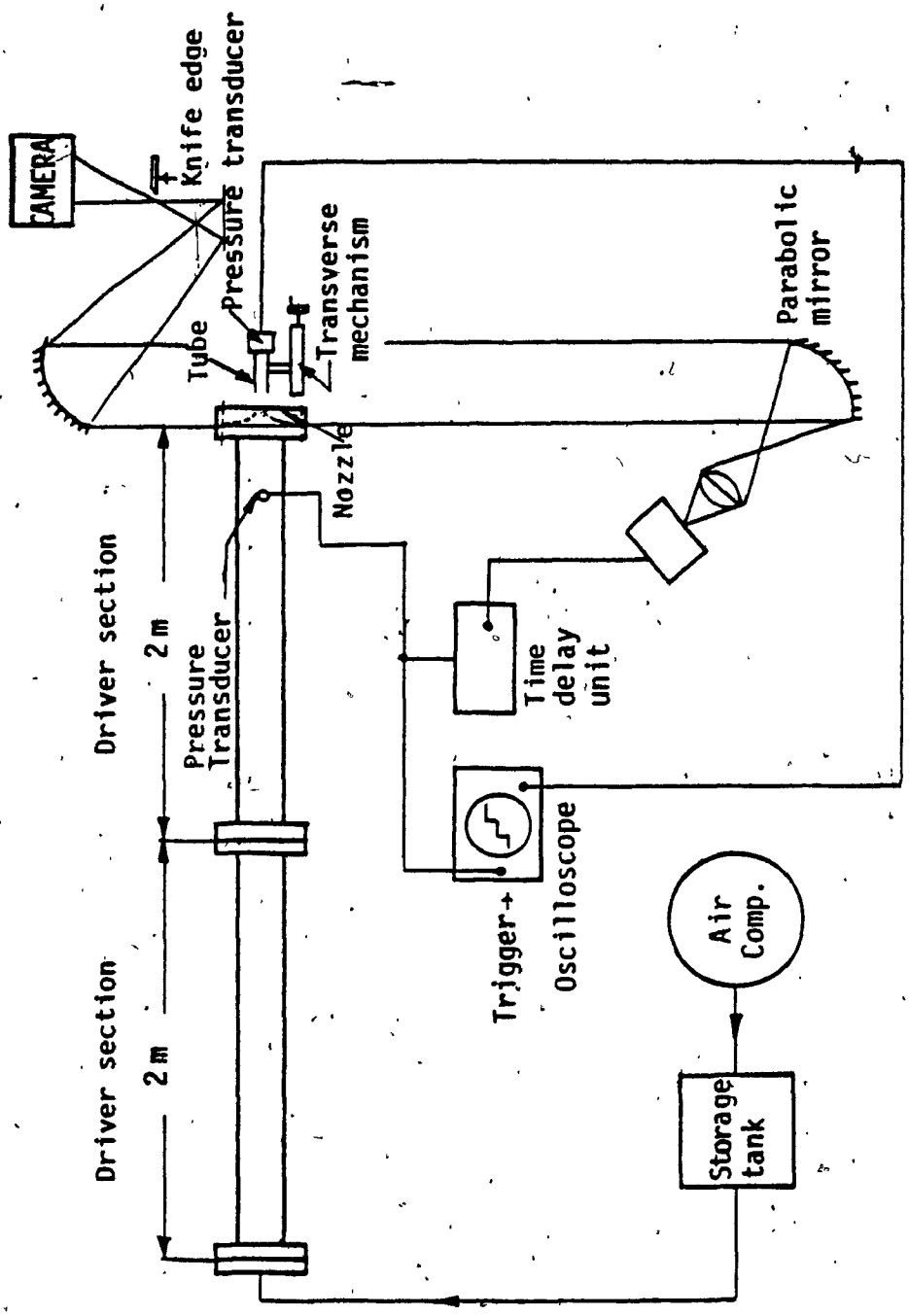


Figure 13. The 50 x 50-mm shock tube and auxiliary equipment

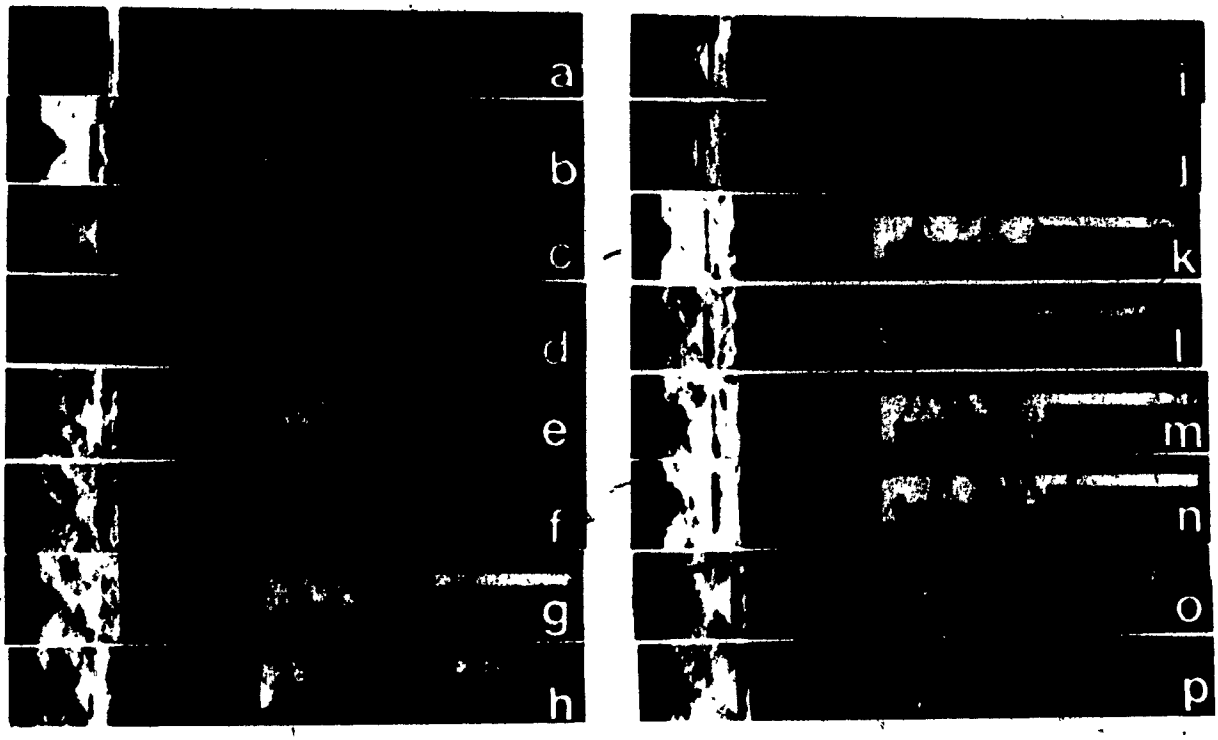


Figure 14. Spark schlieren photograph

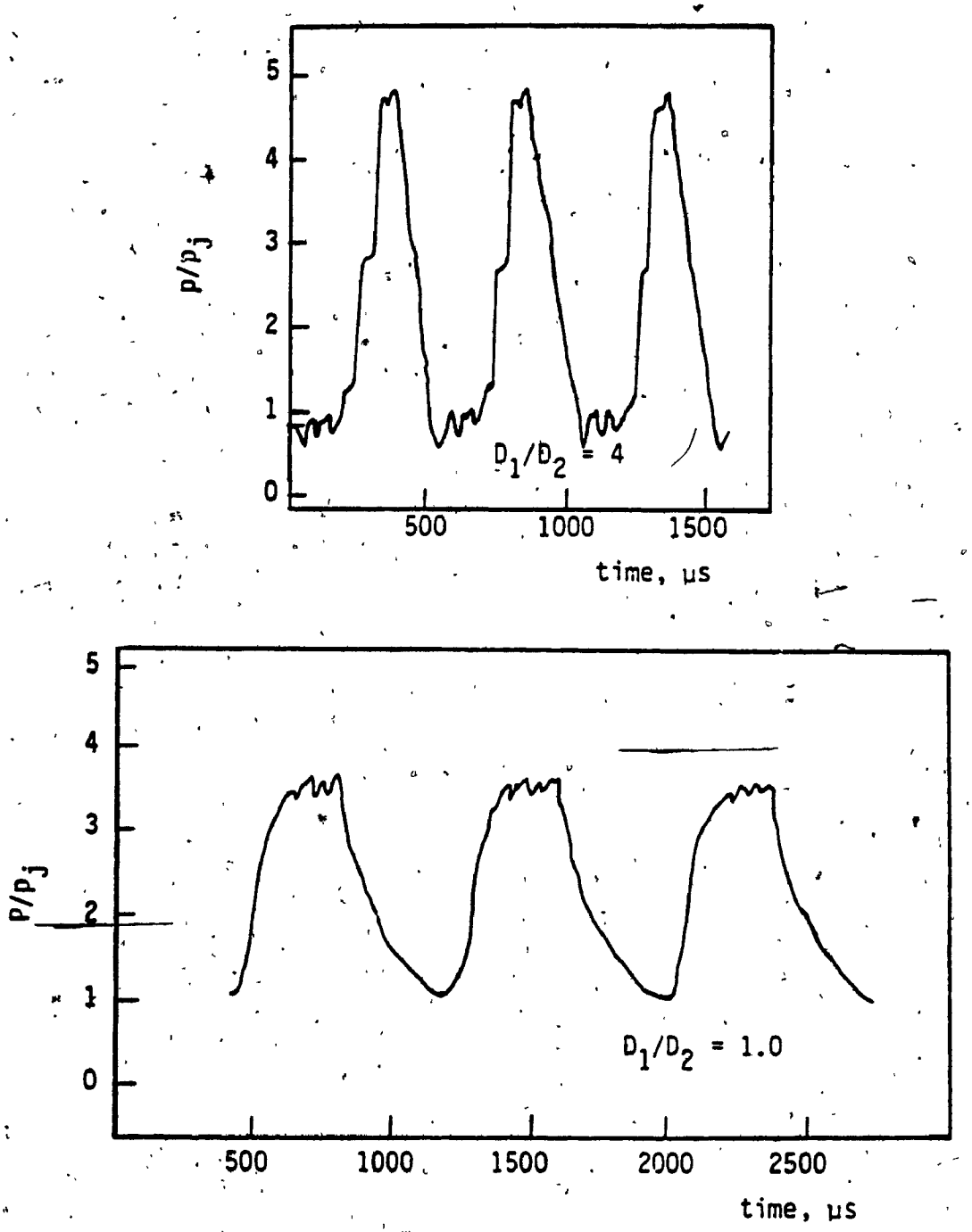


Figure 15. Pressure history for the tube with the area contraction and for the constant area one

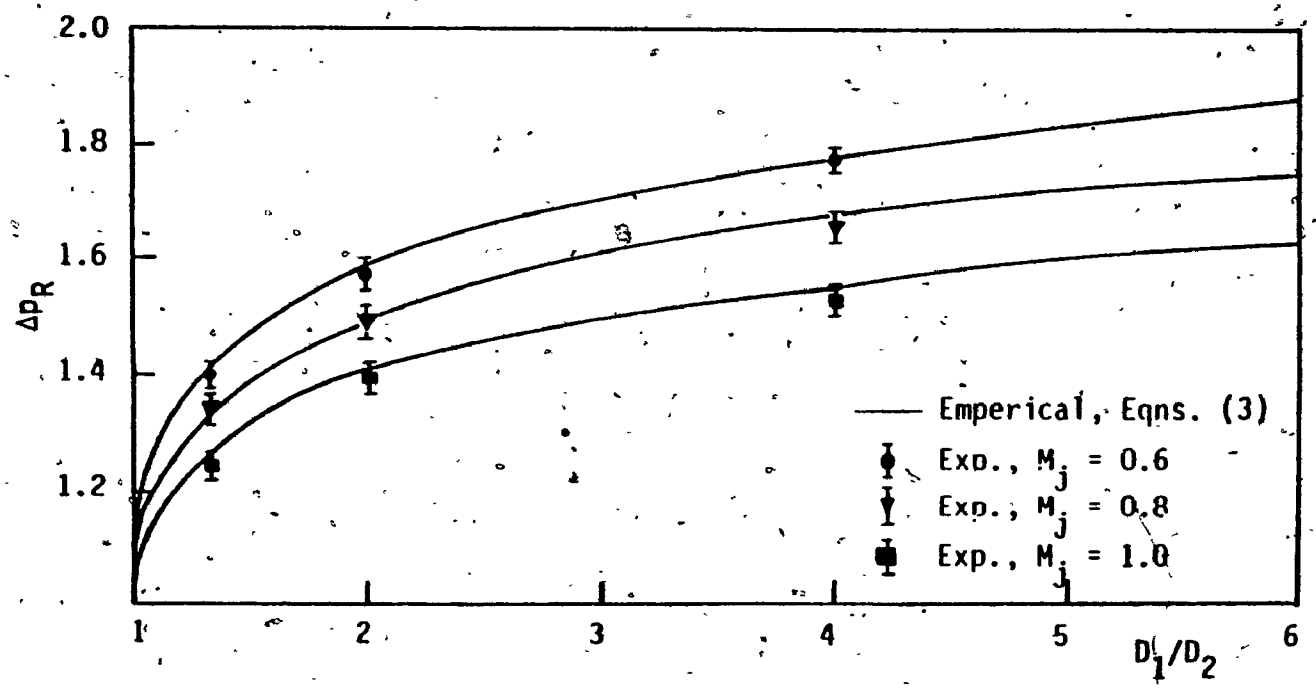


Figure 16. Pressure amplitude as a function of the diameter ratio $D_1/D_2$ for different jet Mach numbers

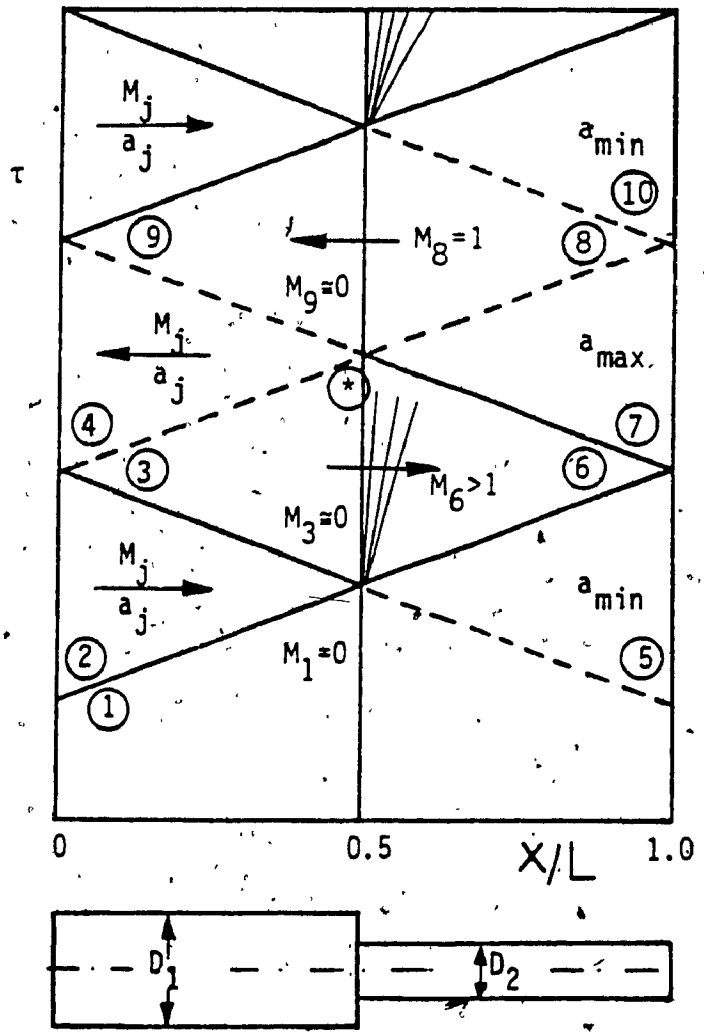


Figure 17. Wave diagram for the large area contraction $D_1/D_2 \to \infty$

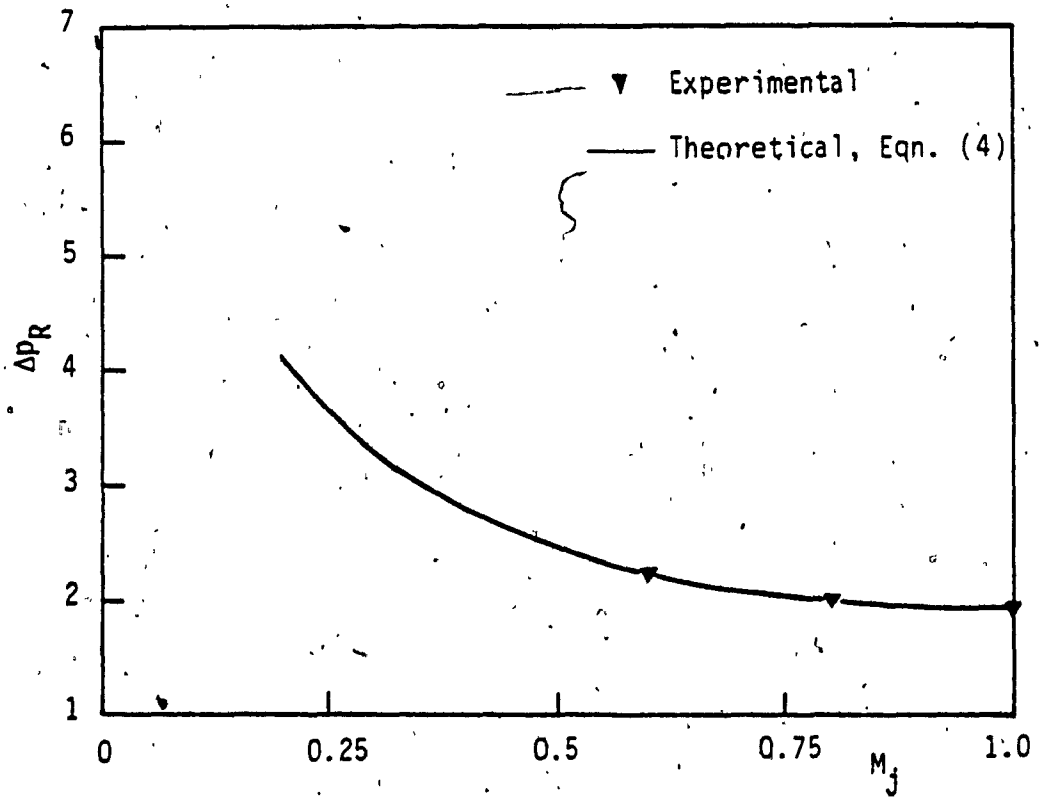


Figure 18. Pressure amplitude as a function of the jet Mach number for the large area contraction, $D_1/D_2 \to \infty$

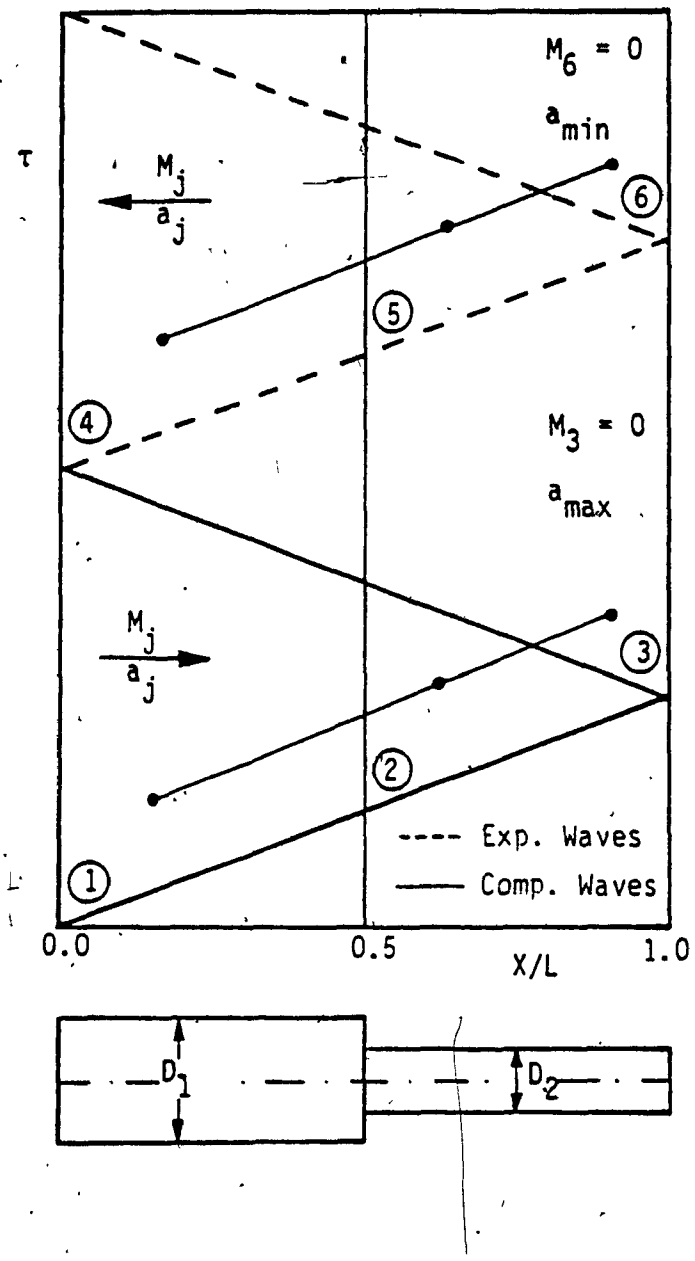


Figure 19. Wave diagram for the small area contraction

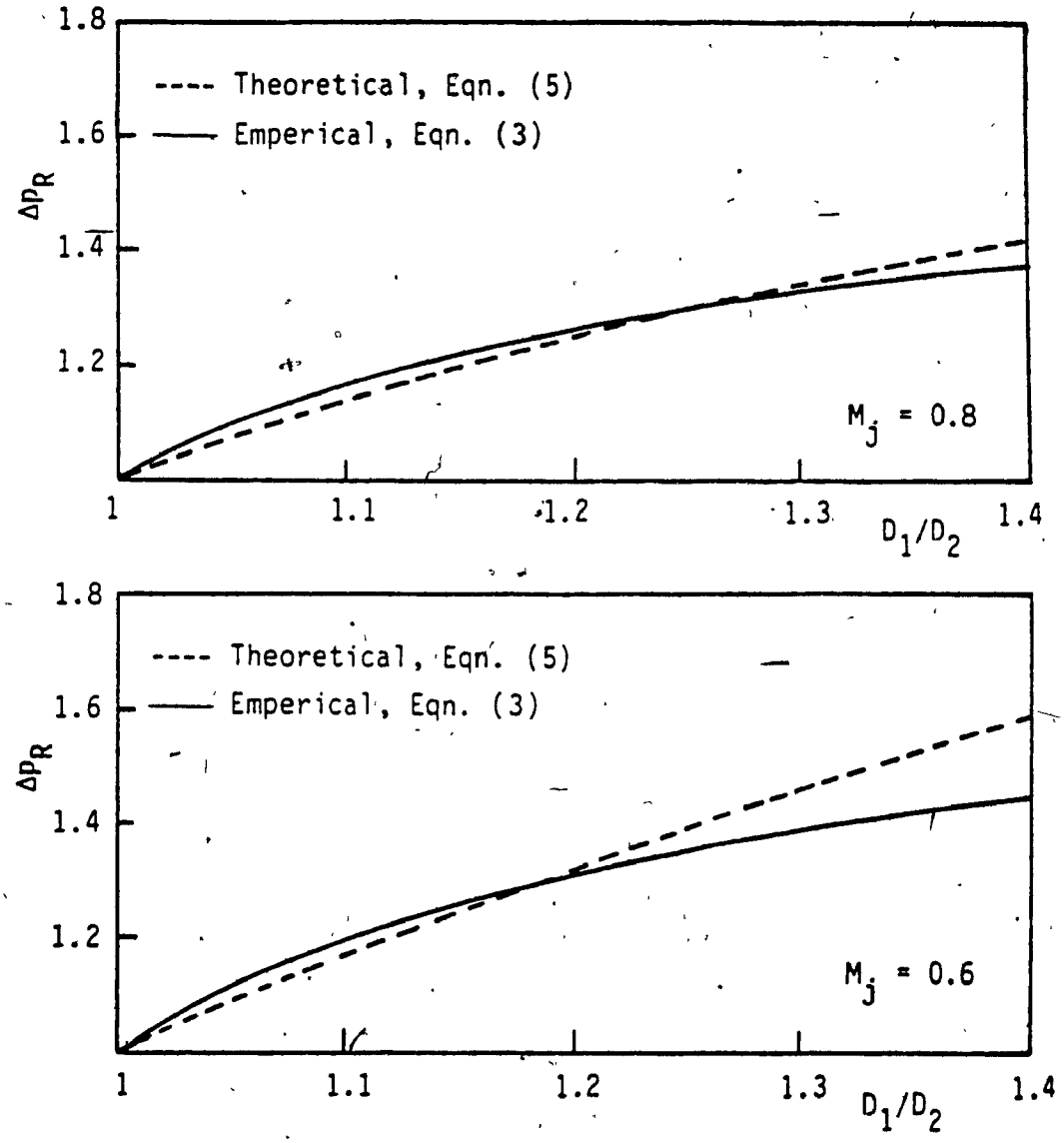


Figure 20. Pressure amplitude as a function of the diameter ratio $D_1/D_2$ for the small area contraction

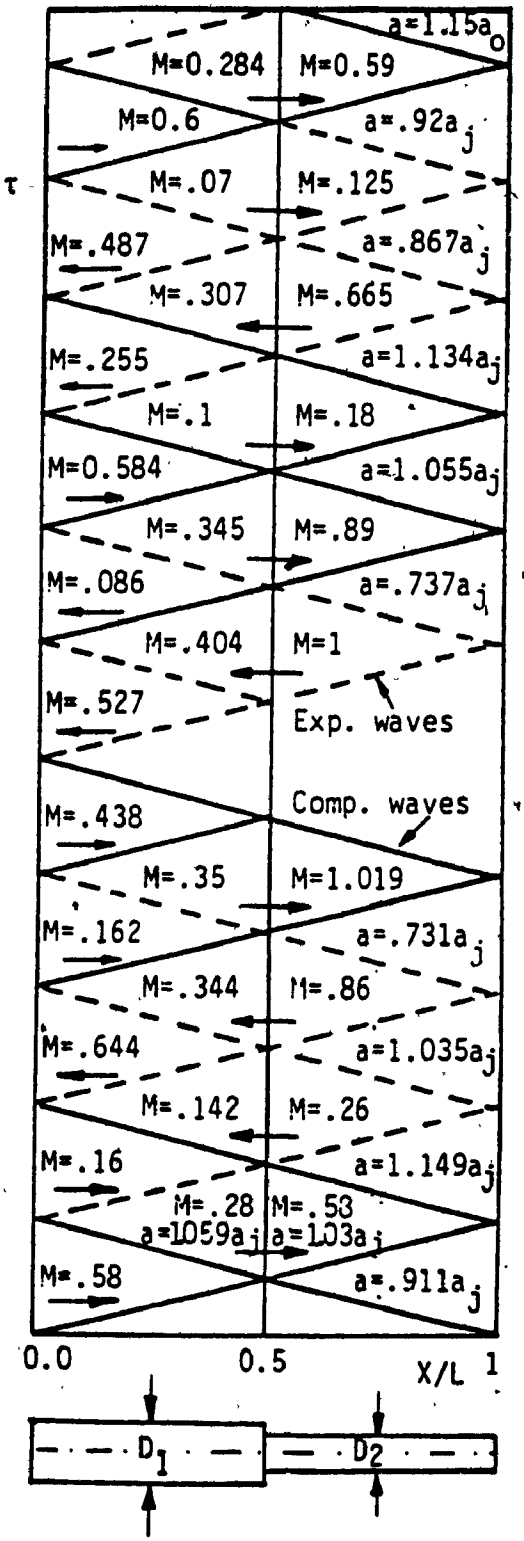


Figure 21. Typical wave diagram for the jet Mach number $M_j = 0.6$ and diameter ratio $D_1/D_2 = 1.33$

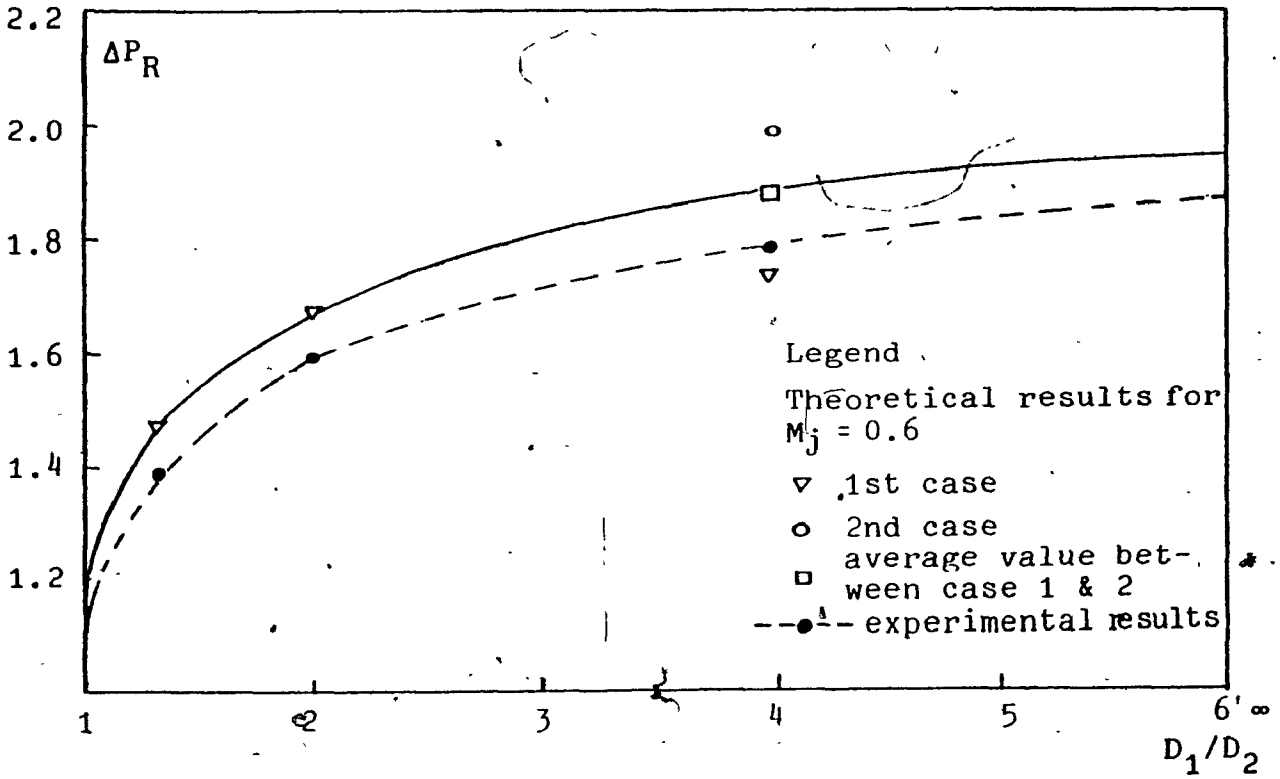


Figure 22. Pressure amplitude as a function of diameter ratio $D_1/D_2$ for $M_j = 0.6$

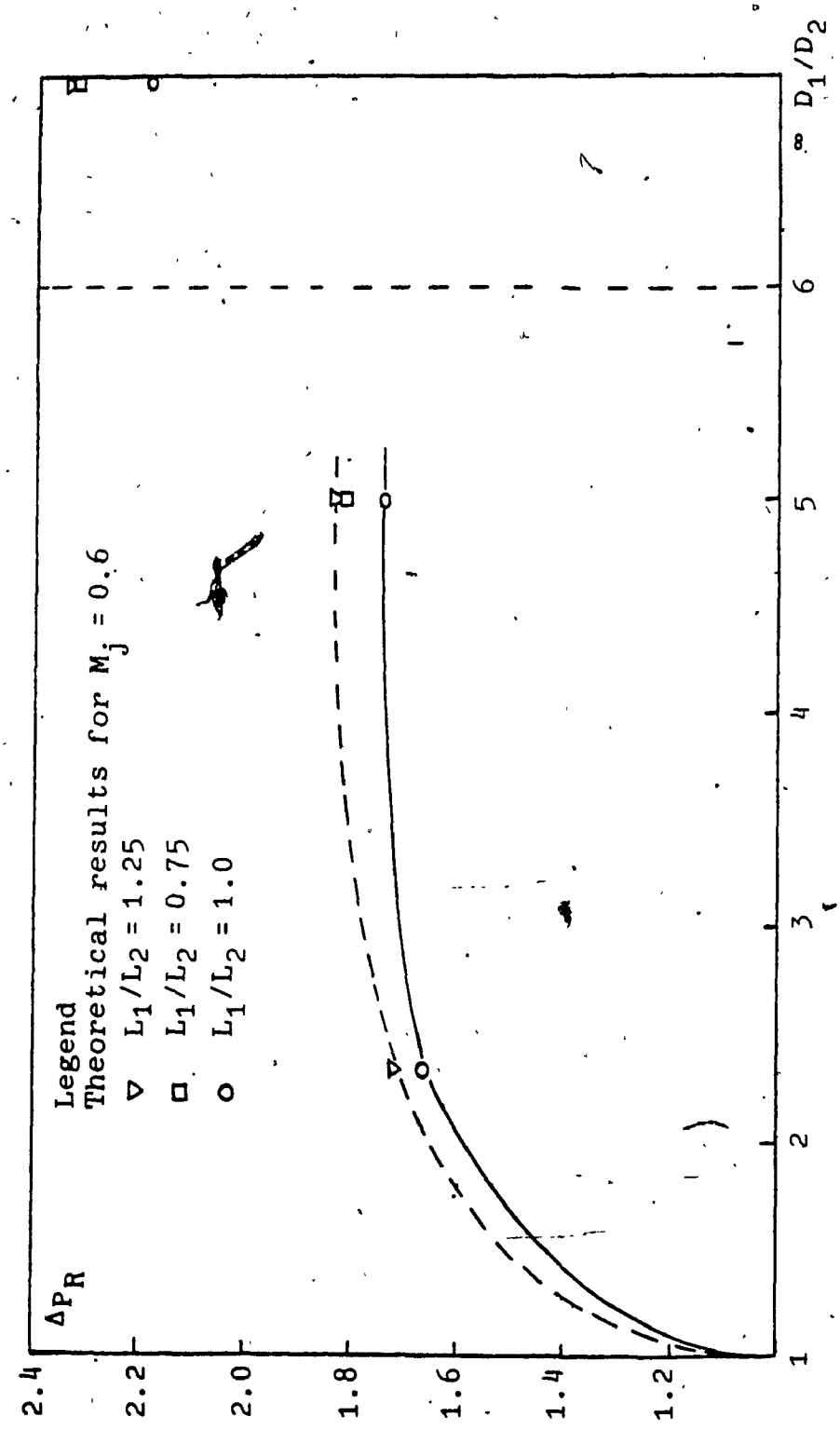


Figure 23. Pressure amplitude as a function of diameter ratio $D_1/D_2$ for different length ratio $L_1/L_2$

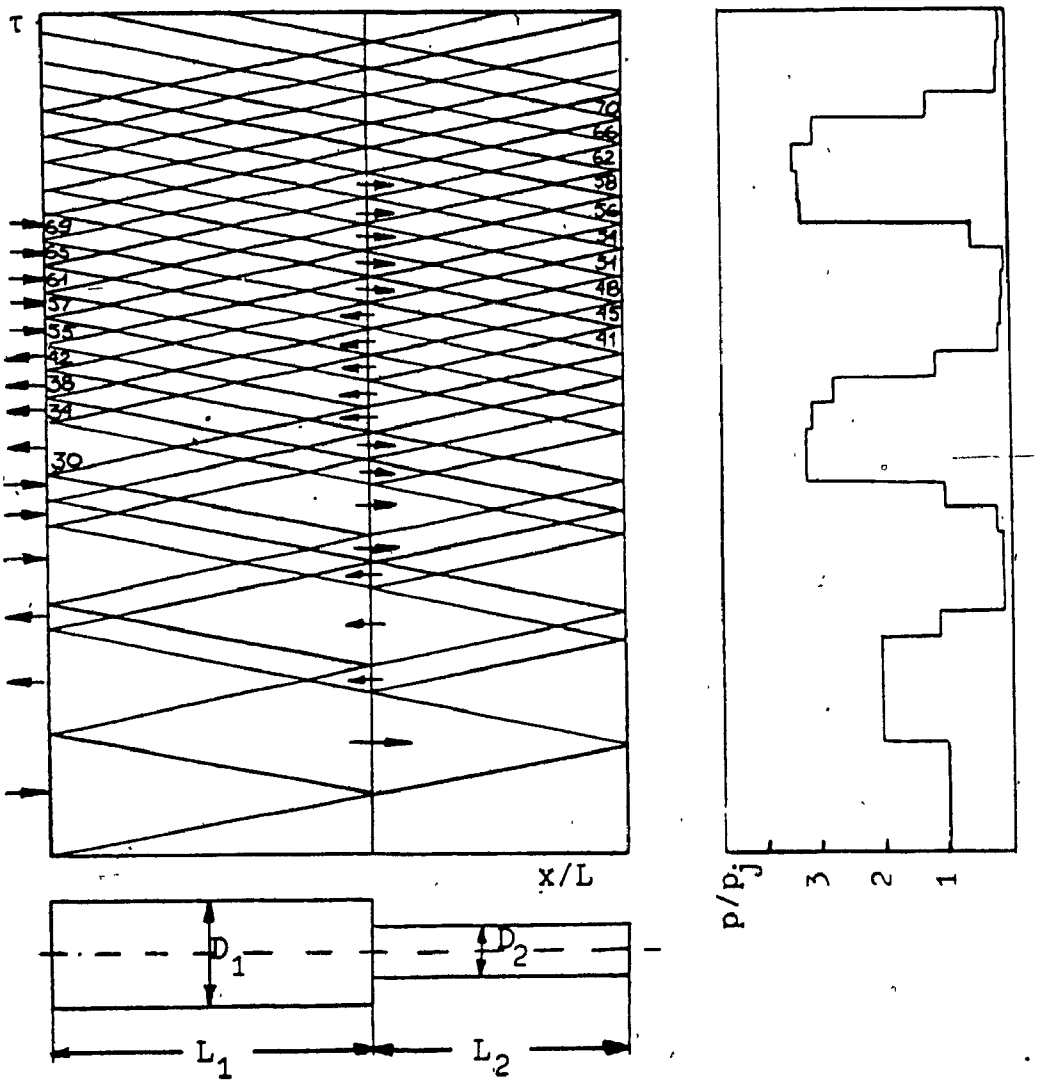


Figure 24. Simplified wave diagram and the pressure history for $M_j = 0.6$, $D_1/D_2 = 4$ and $L_1/L_2 = 1.25$

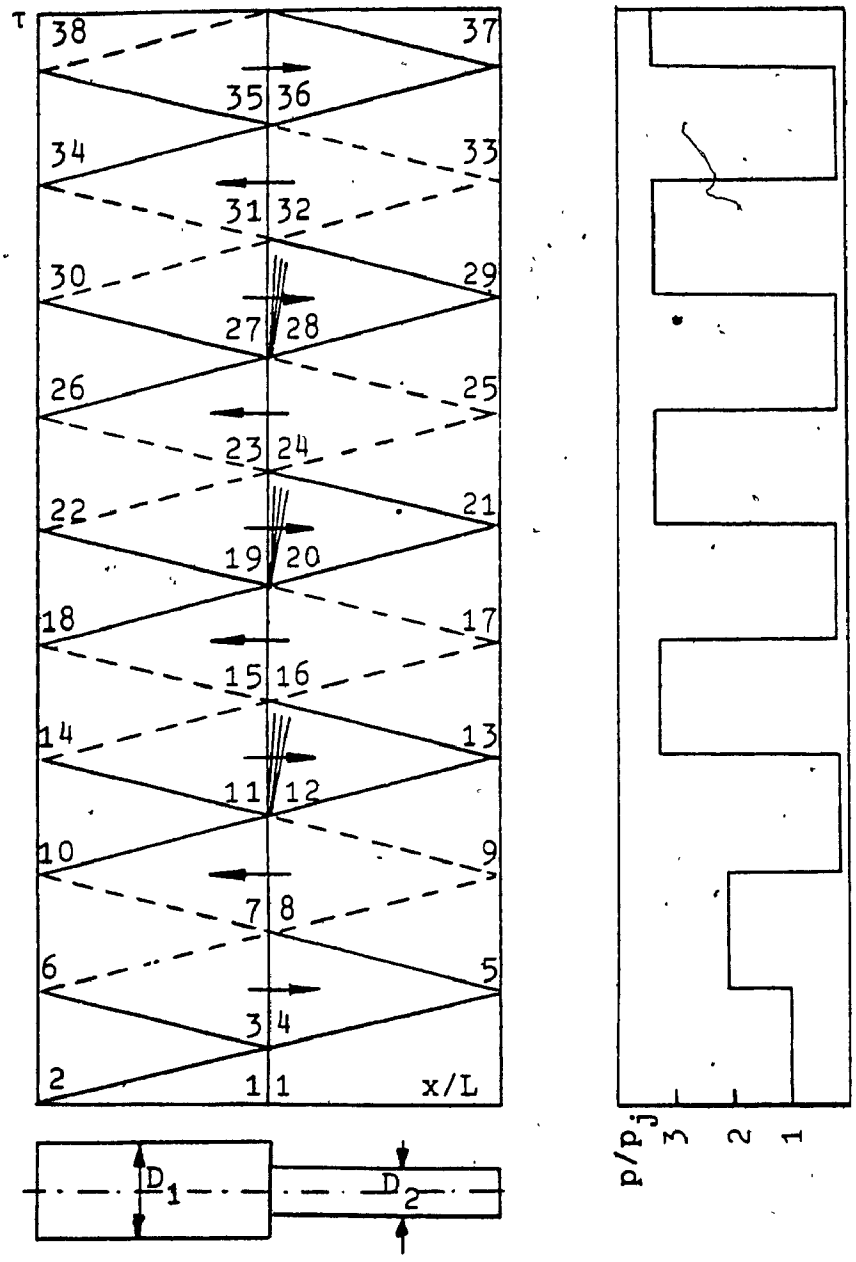


Figure 25. Simplified wave diagram and the pressure history for $M_j = 0.6$, $D_1/D_2 = 4$ and $L_1/L_2 = 1$

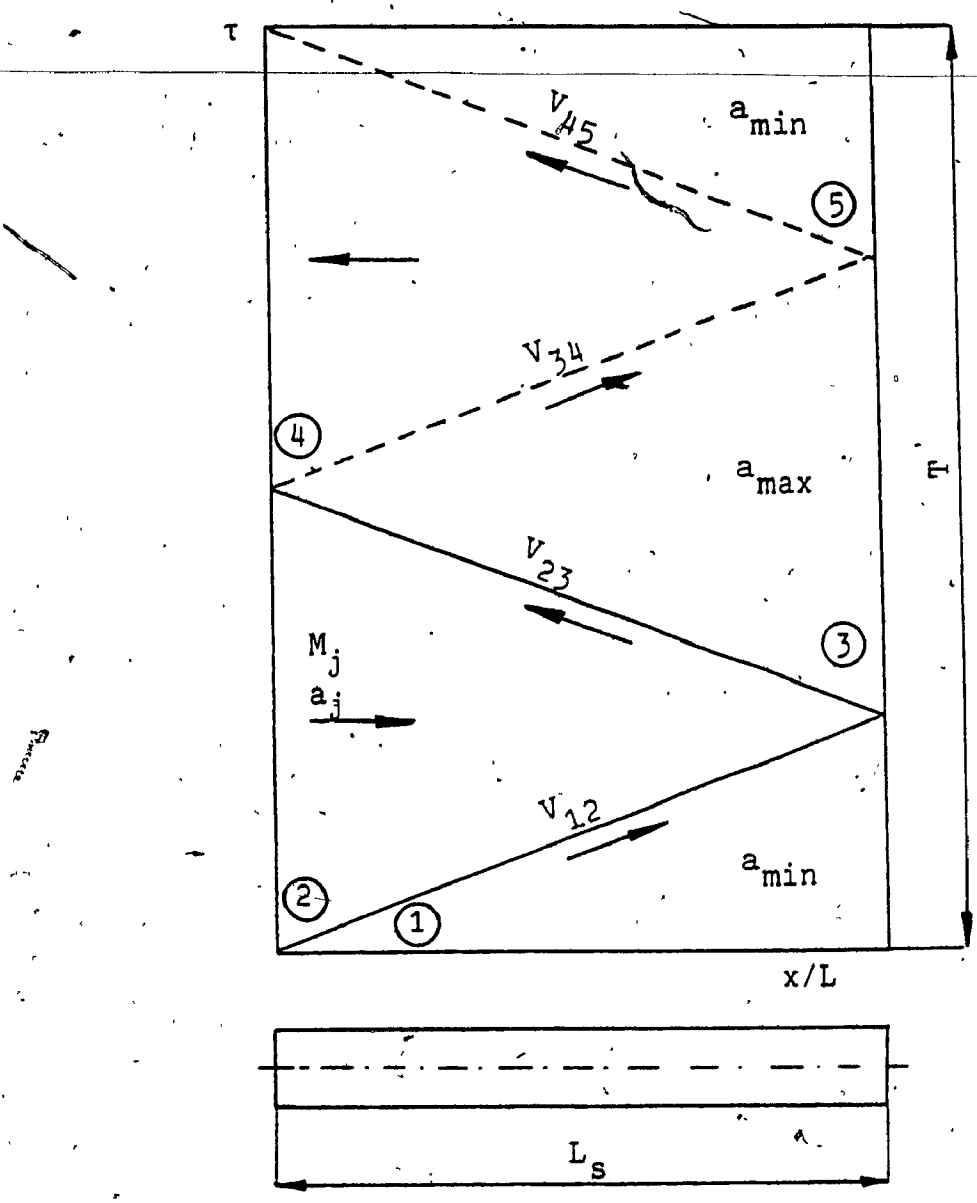


Figure 26. Wave diagram for frequency calculation for the simple tube

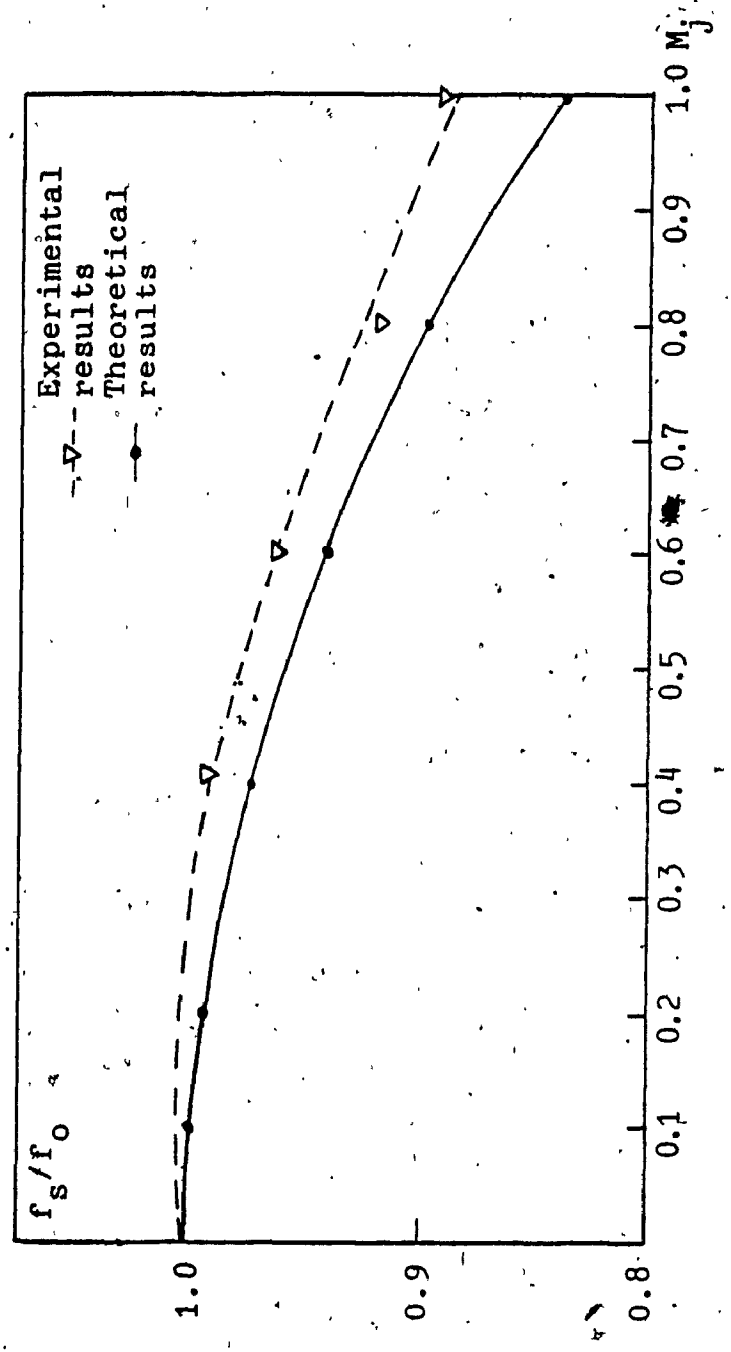


Figure 27. Frequency of oscillations vs. jet Mach number $M_j$

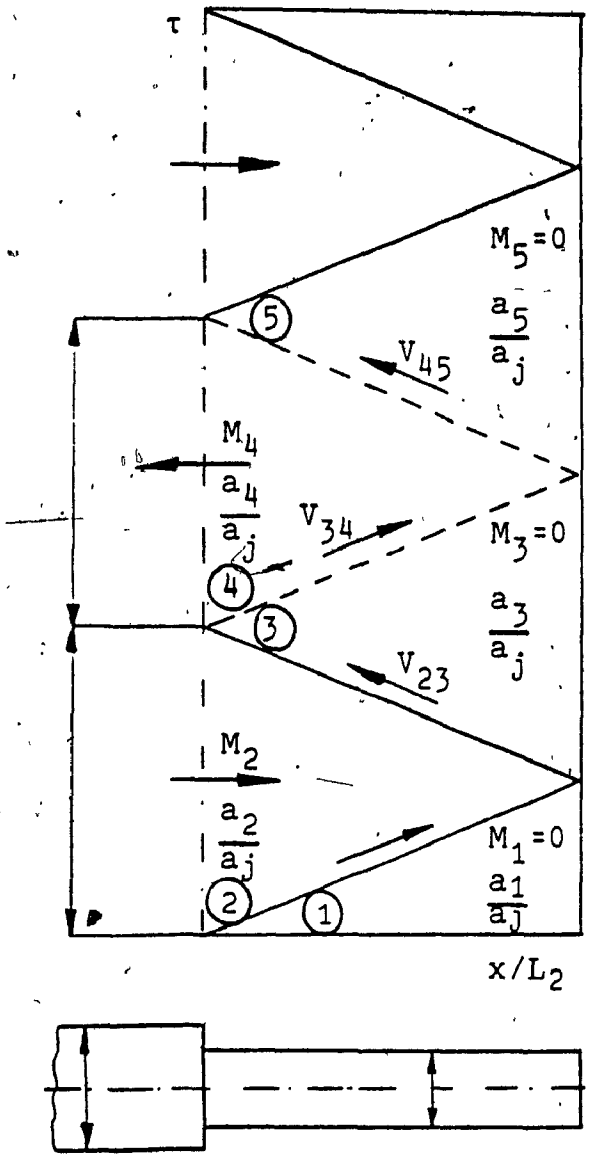


Figure 28: Wave diagram for frequency calculation for the stepped tube

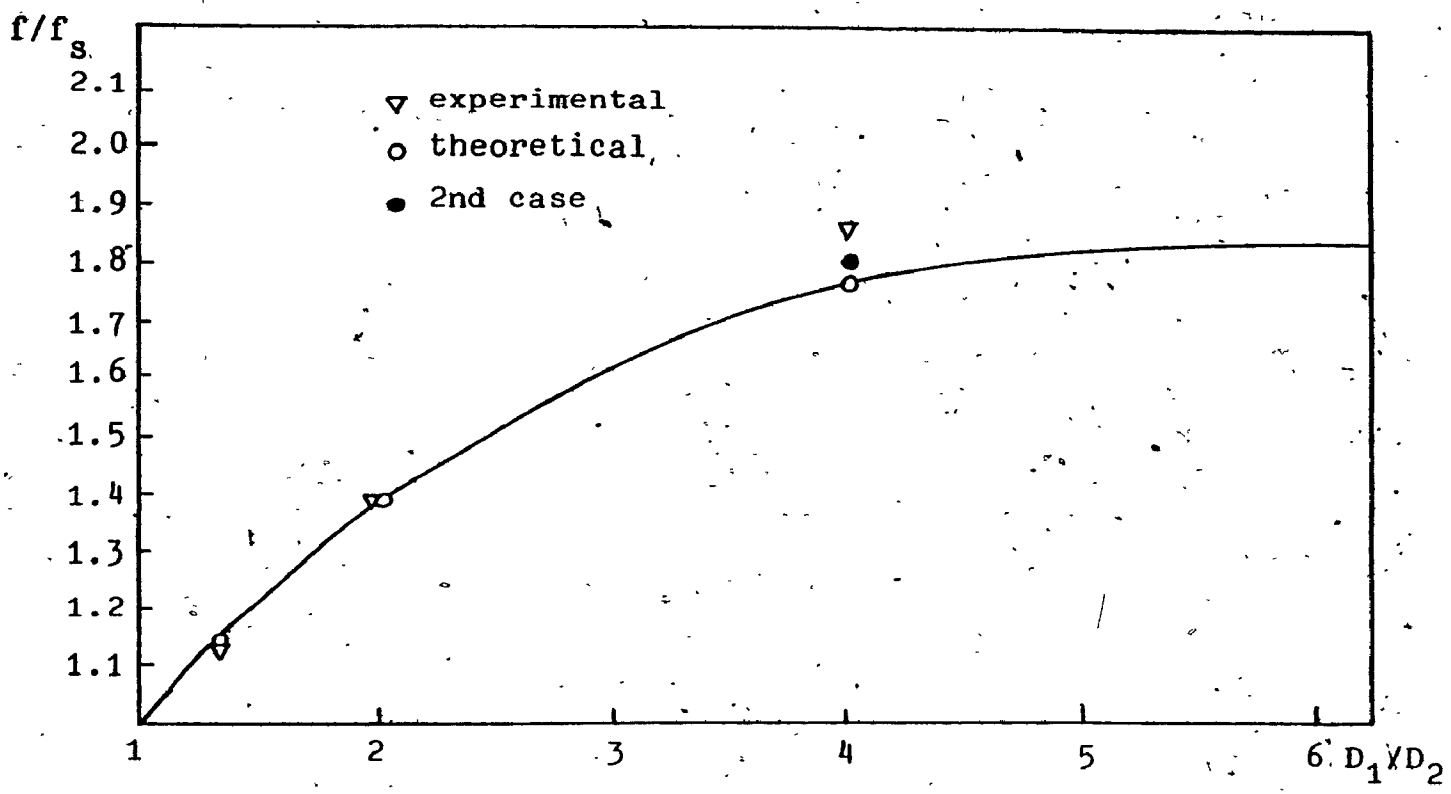


Figure 29. Frequency of oscillations vs. diameter ratio $D_1/D_2$ for the stepped tube

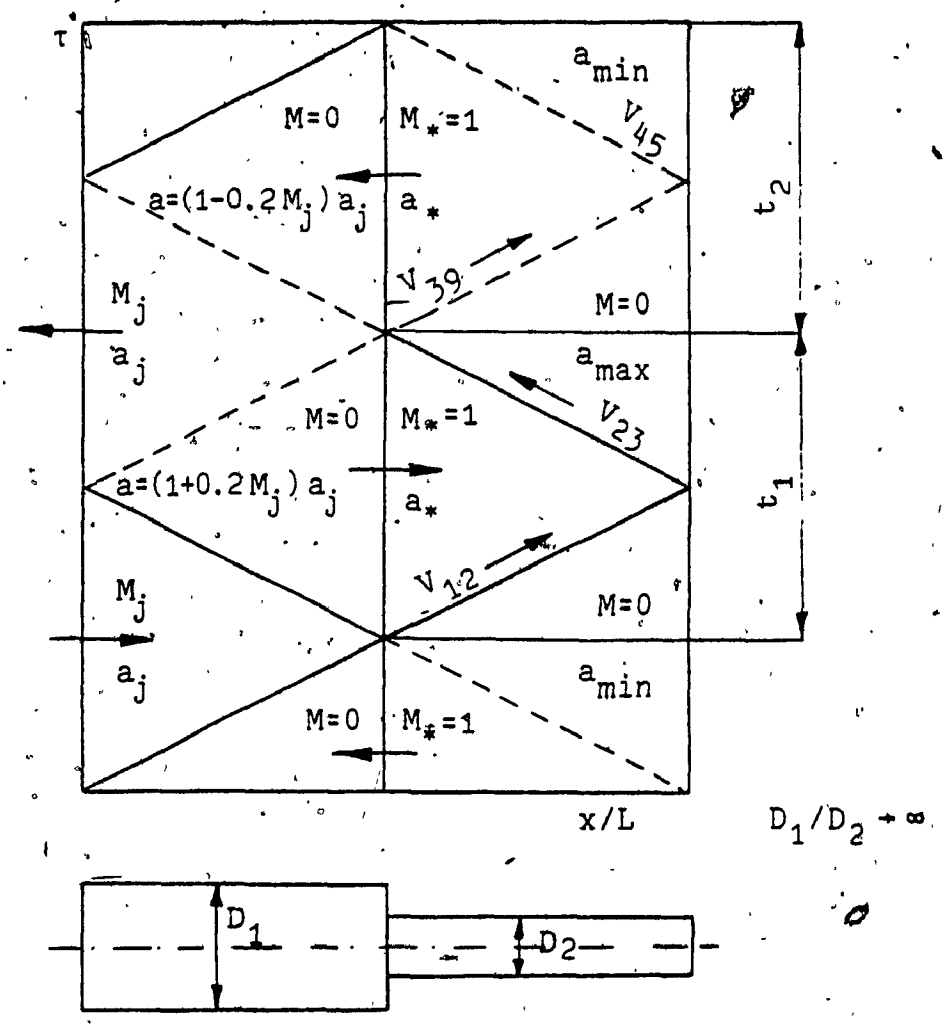


Figure 30. Wave diagram for frequency calculation for tube with large area contraction

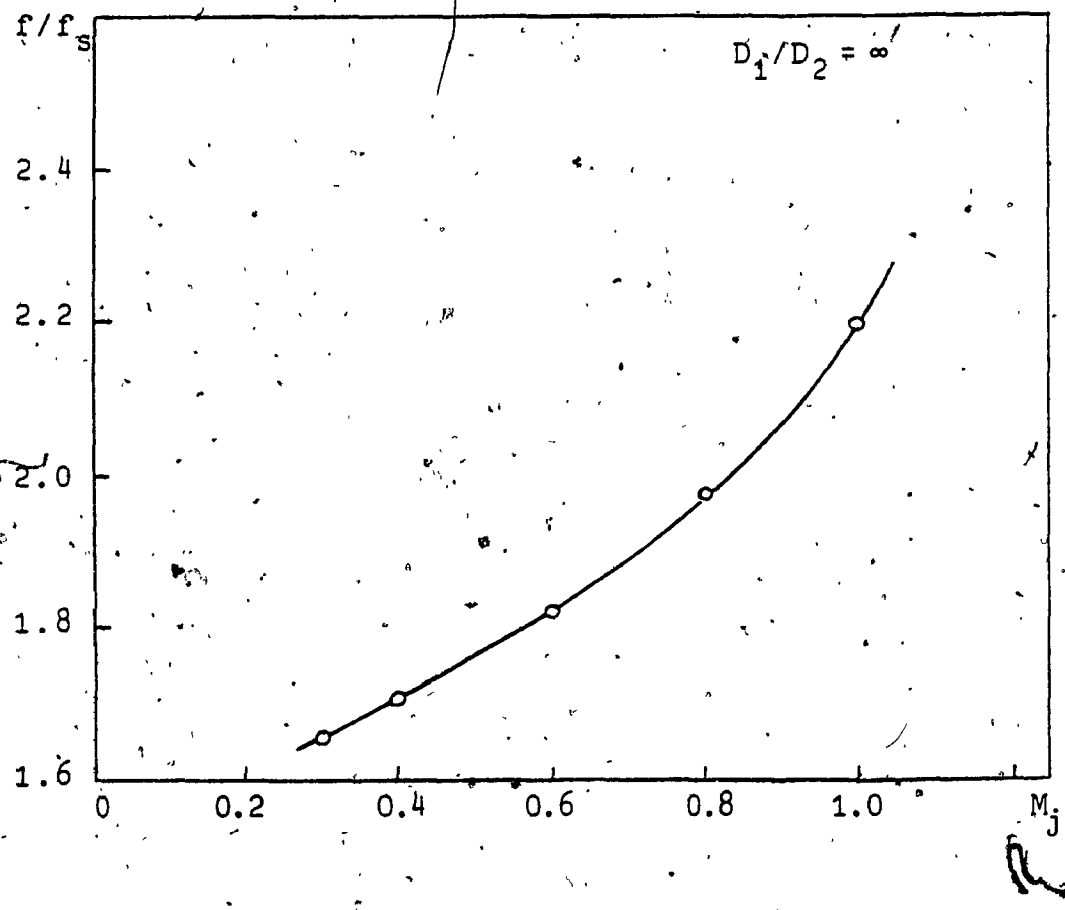


Figure 31. Frequency of oscillations vs. jet Mach number Mj for the tube with large area contraction

Table 1. The Pressure Amplitude for Different Area Ratios and Different Jet Mach Numbers

| $\Delta p_R$ | | | |
|---|---|---|---|
| $M_j$ \ $D_1/D_2$ | 1.34 | 2 | 4 |
| 0.6 | 1.4068 | 1.5932 | 1.7797 |
| 0.8 | 1.3390 | 1.4976 | 1.6656 |
| 1.0 | 1.2710 | 1.4019 | 1.5514 |

Table 2. The Pressure Amplitude as a Function of Diameter Ratio for $M_j = 0.6$

| | $D_1/D_2$ | $\Delta p/p_j$ | $\Delta p_R$ |
|---|---|---|---|
| | 1.333 | 2.634 | 1.462 |
| | 2.000 | 3.006 | 1.668 |
| Case 1 | 4.000 | 3.146 | 1.746 |
| Case 2 | 4.000 | 3.598 | 1.997 |

(for the simple tube and $M_j = 0.6$, $\Delta p/p_j = 1.802$)

Table 3. The Pressure Amplitude as a Function of Length Ratio for Different Diameter Ratios and $M_j = 0.6$

| $\Delta p_R$ | | | |
|---|---|---|---|
| $D_1/D_2$ | $L_1/L_2 = 1$ | $L_1/L_2 = 0.75$ | $L_1/L_2 = 1.25$ |
| 2 | 1.668 | -- | 1.740 |
| 4 (*) | 1.746 | 1.819 | 1.837 |
| | 2.180 | 2.260 | 2.269 |

(*)-Case 1

Table 4. The Values of Flow Mach Number and Sound Speed for $M_j = 0.6$, $D_1/D_2 = 4$, $L_1/L_2 = 1.25$ (Figure 24)

| CLOSED END (M = 0). | | | OPEN END | | |
|---|---|---|---|---|---|
| Point | $a/a_j$ | $p/p_j$ | Point | $M_j$ | $a/a_j$ |
| 41 | 0.788 | 0.188 | 30 | -0.352 | 1.000 |
| 45 | 0.783 | 0.181 | 34 | -0.354 | 1.000 |
| 48 | 0.769 | 0.159 | 38 | -0.428 | 1.000 |
| 51 | 0.682 | 0.068 | 42 | -0.600 | 1.000 |
| 54 | 0.932 | 0.612 | 55 | +0.318 | 1.025 |
| 56 | 1.186 | 3.295 | 57 | +0.322 | 1.025 |
| 58 | 1.186 | 3.310 | 61 | +0.338 | 1.024 |
| 62 | 1.190 | 3.385 | 65 | +0.423 | 1.015 |
| 66 | 1.172 | 3.039 | 69 | +0.600 | 1.000 |
| 70 | 1.035 | 1.272 | | | |

Table 5. The Values of Flow Mach Number and Sound Speed for $M_j = 0.6$, $D_1/D_2 = 4$, $L_1/L_2 = 1$ (Figure 25)

| CLOSED END (M = 0) | | | OPEN END | | |
|---|---|---|---|---|---|
| Point | $a/a_j$ | $p/p_j$ | Point | $M_j$ | $a/a_j$ |
| 21 | 1.187 | 3.322 | 18 | +0.329 | 1.014 |
| 25 | 0.791 | 0.194 | 22 | -0.380 | 1.000 |
| 29 | 1.188 | 3.340 | 26 | +0.333 | 1.024 |
| 33 | 0.792 | 0.195 | 30 | -0.382 | 1.000 |
| 37 | 0.188 | 3.340 | 34 | +0.336 | 1.024 |
| | | | 38 | -0.387 | 1.000 |
| | | | AREA CONTRACTION | | |
| | | | 31 | -0.085 | 0.940 |
| | | | 32 | -1.000 | 0.990 |
| | | | 35 | +0.0368 | 1.085 |
| | | | 36 | +1.000 | 0.990 |

Table 6. Frequency of Oscillations for the Simple H-S Tube and Different Jet Mach Numbers

| $M_j$ | 0.1 | 0.2 | 0.4 | 0.6 | 0.8 | 1.0 |
|---|---|---|---|---|---|---|
| $f_s \frac{L_2}{a_j}$ | 0.1248 | 0.1242 | 0.1218 | 0.1178 | 0.1122 | 0.1050 |
| $f_s/f_0$ theory | 0.9984 | 0.9936 | 0.9744 | 0.9424 | 0.8976 | 0.8400 |
| $f_s/f_0$ experiment | -- | -- | 0.9950 | 0.9640 | 0.9190 | 0.8920 |

where $f_0 = \frac{a_j}{8 L_s}$ acoustical frequency of oscillation for the simple tube

Table 7. Frequency of Oscillations for $M_j = 0.6$ and Different Diameter Ratios, $L_1/L_2 = 1$

| $D_1/D_2$ | 1.333 | 2 | 4 | ∞ |
|---|---|---|---|---|
| THEORETICAL $f/f_s$ | 1.1431 | 1.3912 | 1.795 ** <br> 1.762 * | 1.9334 |
| EXPERIMENTAL $f/f_s$ | 1.1287 | 1.3948 | 1.8652 | |

* 1 Case

** 2 Case

Table 8. Frequency of Oscillation for Different Mach Numbers and Large Area Contraction, $D_1/D_2 \to \infty$

| $M_j$ | 0.3 | 0.4 | 0.6 | 0.8 | 1.0 |
|---|---|---|---|---|---|
| $f / f_s$ | 1.649 | 1.700 | 1.823 | 1.982 | 2.190 |